Robust internal model-based voltage control for DC microgrids

An LMI-based H∞ control

Basati, Amir; Guerrero, Josep M.; Vasquez, Juan C.; Fakharian, Ahmad; Johansson, Karl Henrik; Golestan, Saeed

Published in:
Sustainable Energy, Grids and Networks

DOI (link to publication from Publisher):
10.1016/j.segan.2023.101094

Publication date:
2023

Document Version
Publisher's PDF, also known as Version of record

Sustainable Energy, Grids and Networks 35 (2023) 101094

Contents lists available at ScienceDirect

Sustainable Energy, Grids and Networks

journal homepage: www.elsevier.com/locate/segan

Robust internal model-based voltage control for DC microgrids: An LMI based H_∞ control

Amir Basati [a,*], Josep M. Guerrero [a], Juan C. Vasquez [a], Ahmad Fakharian [b], Karl Henrik Johansson [c], Saeed Golestan [a]

[a] Center for Research on Microgrids (CROM), AAU Energy, Aalborg University, Aalborg, Denmark
[b] Department of Electrical Engineering, Qazvin Branch, Islamic Azad University, Qazvin, Iran
[c] Division of Decision and Control Systems, School of Electrical Engineering and Computer Science, KTH Royal Institute of Technology, and Digital Futures, Stockholm, Sweden

ARTICLE INFO

Article history:
Received 25 October 2022
Received in revised form 29 April 2023
Accepted 30 May 2023
Available online 14 June 2023

Keywords:
DC microgrids
DC–DC converter
Internal model control
Voltage control
Robust H_∞ control

ABSTRACT

This paper aims to design a robust internal model-based voltage control (RIMVC) scheme for DC Microgrids (DCMGs) in the presence of unknown external disturbances. Maintaining voltage reference tracking under measurement noise, delays, model parameter uncertainties and unknown external disturbances while the load changes simultaneously is a severe challenge for the DC–DC converters in DCMGs. By developing a modified internal model-based voltage control for DC–DC converters, this work proposes a plug-and-play (PnP) robust voltage control scheme to address the abovementioned challenge. The proposed control method has a cascade structure. In the first step, a modified IMC control is designed to achieve desired tracking performance for a nominal dynamical system. In the next step, the output feedback H_∞ control part is added to improve the performance robustness under external disturbances and parameter uncertainties. The efficiency of the proposed control scheme is evaluated using a real-time MATLAB/Simulink testbed, taking into account unknown internal and external disturbances under various rapid voltage reference changes, model parameter uncertainties, constant power loads, system delays and normal load profile changes in multiple case study scenarios.

1. Introduction

Recently, with the increasing penetration of distributed generators (DGs), Microgrids (MGs) are being seen as a viable solution for fitting these DGs into modern power grids. Moreover, utilizing DCMGs due to their capability to integrate not only with the renewable energy sources but also with most of the typical DC loads as well as by preventing unnecessary AC/DC or DC/AC conversion stages compared to AC Microgrids (ACMGs), is gaining more popularity in both industries and research communities [1,2]. The increasing popularity of DC systems can be attributed to a number of factors, including the maturity of technological advances in DC–DC converters and the proliferation of DC renewable energy sources (e.g., PV panels), energy storage systems (e.g., batteries), and DC loads (e.g., LEDs and electric vehicles) [3,4]. Besides, the lower complexity of control objectives in DCMG systems due to the absence of reactive power flow and frequency synchronization issues provides an opportunity to address some of the other microgrid control challenges compared to ACMG systems. The resilience performance in the presence of numerous unknown external disturbances, measurement noises and control loop delays are the other challenges of voltage stabilization in DCMG systems [5,6].

The common trend in designing DCMGs' control system is the distributed concept, which relies on transferring information between adjacent generation units. In recent years, various distributed control schemes with hierarchical structures including primary, secondary, and tertiary levels have been proposed in the literature [7,8]. Due to the greater importance and efficiency in attaining the required control objectives, most recently published DCMG control schemes focus mainly on the tertiary or secondary levels issues. [9–11]. For instance, power management between multiple MG clusters, economic dispatch and energy management systems is implemented at the tertiary level. Moreover, voltage restoration and power-sharing objectives are considered at the secondary level. Finally, a local controller with a cascade structure is used at the primary level to regulate the output voltage within an acceptable range by following the received voltage set-points from the secondary controller and to share the output current among the units effectively [12].

Generally, DC–DC converters in DCMGs can be controlled in two modes, voltage control or current control. In voltage and current control modes, converters act as a controllable voltage

* Corresponding author.
E-mail address: amba@energy.aau.dk (A. Basati).

https://doi.org/10.1016/j.segan.2023.101094

source to keep the output voltage within an acceptable range or as a controllable current source by controlling the current to meet the specified power reference, respectively [13].

In the primary level of power systems, both droop-based and non-droop-based control techniques are commonly used to achieve the desired objectives of the primary controllers. While the majority of these techniques have decentralized structures [14,15], the rapid advancements in communication network technologies have led to the popularity of distributed architectures that rely on communication links [16]. However, there are concerns about the security of information transmitted via these communication links in the cyber layer, which is crucial for precise controller operation [17]. Despite this, some voltage control methods, like those proposed in [18–21], leverage the advantages of decentralized structures, including scalability and plug-and-play (PnP) functionality, by using distributed architectures. Nevertheless, other critical challenges, such as maintaining system performance within acceptable limits in the presence of internal and external disturbances, measurement noises, and model uncertainties and delays, have received little attention.

In practice, DG units are encountered some time-varying or unknown external disturbances [22]. Moreover, the MG's stability may be degraded or even destroyed if no action is taken against the presence of external disturbances [23]. Different control approaches have been explored and implemented for these purposes recently. For example, in [15], a state-dependent riccati equation-based optimal control is proposed for stabilization and online reference tracking by considering the system's nonlinearities. In addition, in [24], a kalman filter-based control strategy is proposed by considering uncertainties in both measurements and models for MGs with battery energy storage systems (BESS). The control scheme's goal is to limit the amount of active and reactive power purchased from the main grid by controlling the BESS's output current. Moreover, sliding-mode control is a well-known control structure for keeping a system resilient to external disturbances by pushing the system's dynamics to move over a preset switching surface with a discontinuous control signal [25]. Although the sliding mode controls proposed for the distributed manner control system perform reasonably well at both the primary and secondary levels, they have some drawbacks, such as chattering phenomena that cause voltage tracking issues in the DCMGs' performance.

Besides, Internal Model-based Control (IMC) is an advanced control structure that fulfills control goals using a mathematical model of the plant under control. IMC has gained significant acceptance in process control systems because of its simplicity, good resilience, faster step response, less overshoot in transient responses, etc. For instance, a two-degree-of-freedom IMC scheme for a DCMG system with unknown external disturbances is proposed in [26]. Although this control system can achieve some of the desired control goals for DCMGs (as discussed in [26]), a modified IMC control is needed to compensate for the shortcomings of standard IMC schemes fully.

This study is motivated by the question of how to improve the previously proposed method's robustness by employing robust control theory to develop an output feedback controller capable of keeping the system's performance within an acceptable range in the presence of modeling errors between the plant's real model and nominal model. One of these issues is the difficulty in maintaining the system output within an acceptable range according to IEEE standards while taking into account some model uncertainties, which are more likely to arise over time due to changes in the converter's parameters, load uncertainties, MG topology changes, and other factors.

To this end, a modified robust IMC scheme for a high-speed yet accurate voltage control of DCMGs is presented in this study. To face this challenging design problem, a cascade control scheme is proposed. In the first step, a modified IMC control is presented to guarantee desired tracking performance for the nominal dynamical system. In the next step, the output feedback H_∞ control part is added in order to improve the robustness in the presence of external disturbances and parameter uncertainties. An inner loop of standard IMC and an outer loop of robust control make up this control system. The internal model controller is designed using the standard IMC design method. Using any conventional robust control approaches, the robust controller can be constructed to ensure robust stability and performance.

An H_∞ robust internal model-based voltage control (RIMVC) is proposed in this paper to ensure not only all of the potential advantages of using conventional voltage controllers, which were unable to eliminate external disturbances, but also to fully remove external disturbances as well as measurement noises and model uncertainties. For designing such a control approach, precise mathematical modeling of the explored MGs is needed. Although the proposed control scheme is located at the lowest level of a hierarchical control structure for DCMGs, it plays a crucial role in a hierarchical control structure. Furthermore, the entire hierarchical control structure is highly dependent on the primary controller's performance, which significantly impacts the control system since they are responsible for achieving some of the most critical DCMGs' desired control goals.

In this study, a DCMG testbed with N units is utilized to validate the efficiency of the proposed control scheme. This MG testbed is designed to take into account a variety of variables such as different MG topologies, load variations, and PnP capabilities. It should be highlighted that these additional achievements, particularly those achieved by modifications to the standard IMC control structure discussed in [26], do not add significant computational costs to the system.

The main contributions of this study include:

- Proposing a fully decentralized and robust internal model-based voltage regulation control scheme that enables precise and stable voltage control.
- Providing plug-and-play (PnP) functionality for all distributed generation (DG) units and the ability to scale up to a high number of units, making the system highly adaptable to changes.
- Proposing a comprehensive resilience control scheme that deals simultaneously with internal and external disturbances, model parameter uncertainties, measurement noise, and system delays in the control loop. This scheme ensures that the system performance remains within acceptable limits even in fast voltage reference changes and load profile variations.

The rest of this paper is organized as follows: Section 2 presents a mathematical model of the DCMG system. In Section 3, a comprehensive description of the proposed Robust IMC technique is presented. The simulation results are represented in Section 4. In addition, a brief discussion is given in Section 5, which is followed by numerical evaluations. Finally, the paper is concluded in Section 6.

2. DC microgrids mathematical model

Fig. 1 depicts the general layout of a DCMG testbed. For the sake of simplicity in modeling, two DG units, i and j, connected through a distribution line consisting of R_{ij} and L_{ij}, are considered. The mathematical equations of the model could change as a result of various DC–DC converter types, such as boost or buck, and so on. Two DC–DC buck converters with suitable R_i, L_i and C_i values, two DC sources V_{dci} and V_{dcj}, and two DC loads represented by two

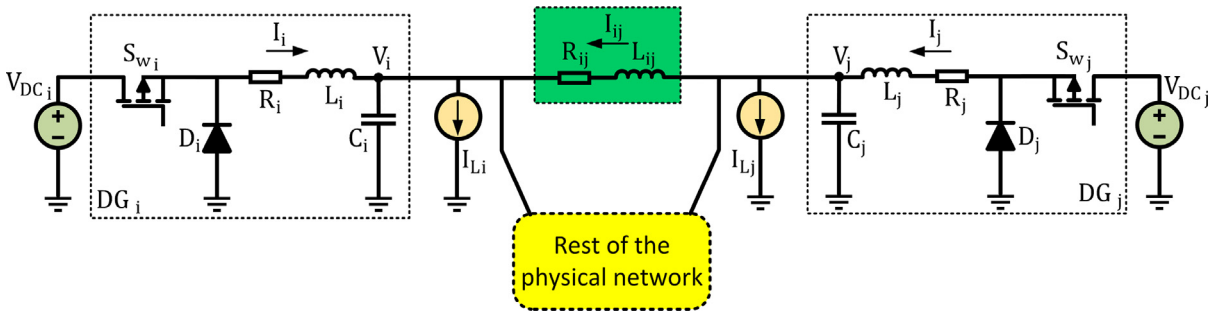

Fig. 1. DCMG configuration in which DG_i is connected to DG_j via a distribution line.

current sources I_{Li} and I_{Lj} are included in the DCMG that is used to derive the mathematical model in this section. Each DG unit is linked to a local load. Each DG unit comprises a DC source coming from the renewable energy source (RES), a DC–DC converter, and a local load with a variety of unknown profiles.

This paper considers a common configuration of a DCMG, which consists of a transistor switch, an RL filter with the parameters R_i, L_i, and a shunt capacitor C_i, based on the presented model in [13].

$$\text{DG}\,i: \begin{cases} \frac{dV_i}{dt} &= \frac{1}{C_i} I_i - \frac{1}{C_i} I_{L_i} + \frac{1}{C_i} I_{ij} \\ \frac{dI_i}{dt} &= -\frac{1}{L_i} V_i - \frac{R_i}{L_i} I_i + \frac{d_{buck_i}}{L_i} V_{dc_i} \end{cases} \tag{1}$$

$$\text{Line}\,ij: \frac{dI_{ij}}{dt} = -\frac{R_{ij}}{L_{ij}} I_{ij} + \frac{1}{L_{ij}} V_j - \frac{1}{L_{ij}} V_i \tag{2}$$

Moreover, based on the [18,27], a quasi stationary model of DCMG with multiple DGs is considered in this study, which means that all distribution lines can be assumed to have quasi-stationary dynamics if the time constant of line transients is extremely fast, meaning that L_i and L_j are significantly small, then line dynamics can be neglected. ($\frac{dI_{ij}}{dt} = 0$). Based on this assumption, (2) may be simplified as:

$$I_{ij} = \frac{V_j - V_i}{R_{ij}} \tag{3}$$

Substituting (3) into (1) gives the governing differential equations of DG_i as:

$$\text{DG}\,i: \begin{cases} \frac{dV_i}{dt} &= \frac{1}{C_{t_i}} I_{t_i} - \frac{1}{C_{t_i}} I_{L_i} + \frac{1}{C_{t_i} R_{ij}} V_j - \frac{1}{C_{t_i} R_{ij}} V_i \\ \frac{dI_{t_i}}{dt} &= -\frac{1}{L_{t_i}} V_i - \frac{R_{t_i}}{L_{t_i}} I_{t_i} + \frac{d_{buck_i}}{L_{t_i}} V_{dc_i} \end{cases} \tag{4}$$

From (4), the state-space equations of the DG_i can be derived as:

$$\begin{bmatrix} \dot{V}_i \\ \dot{I}_i \end{bmatrix} = \begin{bmatrix} -\sum_{j\in N_i} \frac{1}{C_i R_{ij}} & \frac{1}{C_i} \\ \frac{1}{L_i} & \frac{R_i}{L_i} \end{bmatrix} \begin{bmatrix} V_i \\ I_i \end{bmatrix} + \begin{bmatrix} -\frac{1}{C_i} & \sum_{j\in N_i} \frac{1}{C_i R_{ij}} & 0 \\ 0 & 0 & \frac{1}{L_i} \end{bmatrix} \begin{bmatrix} I_{L_i} \\ V_j \\ d_{buck_i} V_{dc_i} \end{bmatrix} \tag{5}$$

$$\begin{bmatrix} y_1 \\ y_2 \\ y_3 \end{bmatrix} = \begin{bmatrix} 1 & 0 \\ 0 & 0 \\ 0 & 0 \end{bmatrix} \begin{bmatrix} V_i \\ I_i \end{bmatrix} + \begin{bmatrix} 0 & 0 & 0 \\ 1 & 0 & 0 \\ 0 & 0 & 1 \end{bmatrix} \begin{bmatrix} I_{L_i} \\ V_j \\ d_{buck_i} V_{dc_i} \end{bmatrix} + \begin{bmatrix} 1 \\ 0 \\ 0 \end{bmatrix} n_i(t) \tag{6}$$

where $\begin{bmatrix} V_i & I_i \end{bmatrix}^T$ are the states, $u_i = d_{buck_i} V_{dc_i}$ is the input, and $n_i(t)$ model unknown external disturbances.

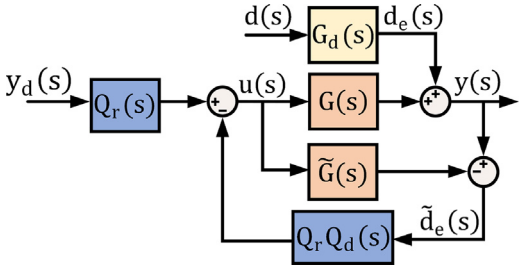

Fig. 2. Structure of internal model control.

Assumption 1. The external disturbance $n_i(t)$, $i \in \{1, 2, \ldots, N\}$, satisfies $|n_i| \leq \rho$ and $|\dot{n}_i| \leq \sigma$, where N indicates the number of DG units, and ρ and σ are positive constants.

The system matrix dimension should be squared for simplicity in the IMC design procedure, and thus the number of inputs and outputs should be equal. Therefore I_{L_i} and V_j are considered as two exogenous inputs that necessitate considering two virtual outputs in output vector $y_i = \begin{bmatrix} V_i & I_{L_i} & d_{buck_i} V_{dc_i} \end{bmatrix}^T$ to keep the system's matrix squared.

3. Proposed RIMVC strategy

This paper proposes a new control design for VSCs based on the modified two degrees of freedom IMC and the H_∞ robust control. The proposed control system includes IMC for voltage regulation by tracking the received secondary controller's set-points and robust control for increasing robustness and enhancing voltage regulation quality in the face of model uncertainties. It is worth mentioning that utilizing a H_∞ robust controller over the modified IMC will have no considerable impact on the computational complexity or dynamic performance of the proposed method.

The design procedure can be summarized as follows:

- Design the modified IMC control to achieve the desired tracking performance, such as a low steady-state tracking error.
- Design the H_∞ control in order to improve the system's tracking performance, disturbance rejection, or robustness.

The modified IMC and H_∞ robust control designing procedures are discussed in the following.

3.1. Proposed modified IMC strategy

The inner loop of the proposed method is a two-degree-of-freedom internal model-based voltage control strategy for DCMGs, as shown graphically in Fig. 2.

The output transfer function for each DG can be expressed as follows:

$$\underbrace{\begin{bmatrix} Y_1(s) \\ Y_2(s) \\ Y_3(s) \end{bmatrix}}_{Y(s)} = \underbrace{\begin{bmatrix} G_{11}(s) & G_{12}(s) & G_{13}(s) \\ G_{21}(s) & G_{22}(s) & G_{23}(s) \\ G_{31}(s) & G_{32}(s) & G_{33}(s) \end{bmatrix}}_{G(s)} \underbrace{\begin{bmatrix} U_1(s) \\ U_2(s) \\ U_3(s) \end{bmatrix}}_{U(s)} + \begin{bmatrix} 0 \\ 0 \\ 1 \end{bmatrix} N_i(s) \tag{7}$$

where, Y_i, U_i, G_{ij} and N_i are the outputs vector, inputs vector, sub-transfer functions and external disturbance for each DG unit, respectively.

Assumption 2. All the elements in $G(s)$ are stable and due to considering an equal number of input and output in the state-space model, then the $G^{-1}(s)$ also exists. Moreover, for a perfect control, a perfect model is needed. To this end it is assumed that the equivalent model of $G(s)$ is also perfect, therefore $\tilde{G}(s) = G(s)$ [28].

For the sake of simplicity in calculation, $G(s)$ could be split into two distinct sub-functions based on minimum phase (MP) and non-minimum phase (NMP) terms, each containing either $G(s)$'s MP or NMP terms. $G_{-}(s)$ is the subsystem containing MP terms, such as the plant's stable poles or zeros, while $G_{+}(s)$ is the subsystem containing NMP terms, such as delays and right-hand side zeros. It should be mentioned that according to the $G(s)$'s right-hand side zeros, equal poles on the left-hand side with the same value as the denominator's zeros should be added to the $G_{+}(s)$. Then, $G(s) = G_{+}(s)G_{-}(s)$, where

$$G_{+}(s) = e^{-\tau s} \prod_i \frac{-\beta_i s + 1}{\beta_i s + 1} \qquad \beta_i > 0 \tag{8}$$

$$G_{-}(s) = G(s)G_{+}^{-1}(s). \tag{9}$$

Also, the updated model transfer function could also be reformulated as follows in the presence of time delay in the system, such as $e^{-\tau s}$, using the first-order Pade approximation:

$$e^{-\tau s} \approx \left(\frac{1 - \frac{\tau}{2}s}{1 + \frac{\tau}{2}s}\right) \tag{10}$$

$$\tilde{G}(s) = G(s)\left(\frac{1 - \frac{\tau}{2}s}{1 + \frac{\tau}{2}s}\right) \tag{11}$$

Based on the proposed control method depicted in Fig. 2, the output expression is as follows:

$$Y(s) = Q_r(s)\tilde{G}(s)Y_d(s) + (1 - Q_r Q_d(s)\tilde{G}(s))G_d(s)D(s) \tag{12}$$

The output expression includes two main components, the first one is used to maintain voltage reference tracking by using the $Q_r(s)$, and the second one is used to maintain disturbance rejection by using the $Q_d(s)$.

Moreover, an ideal IMC controller can be designed if $G(s)$ is perfect and it has the inverse model, but since the inertial element and integration element are always present in the process, the inverse model will be challenging to achieve in practice. To address this issue, a filter such as $F(s)$ is needed to ensure robustness to the modeling mismatches as well as stability, in the presence of a mismatch between the $G(s)$ and the $\tilde{G}(s)$ [28]. Based on [6], the closed-loop stability can be guaranteed for any mismatch by selecting large enough constants for the filter. The filter equation is represented below:

$$F(s) = \frac{as + b}{(1 + \lambda s)^n} \tag{13}$$

where a, b, λ, and n should be calculated in such a way that the ramp changes reference tracking error becomes zero and the value of n must be chosen such that $Q_r(s)$ could be a proper transfer function, as well [29].

$$a = \frac{(\lambda_n G_{+}(0) - \frac{dG_{+}(0)}{ds})}{G_{+}^2(0)} \tag{14}$$

$$b = G_{+}^{-1}(0) \tag{15}$$

Finally, the expressions for the $Q_r(s)$ and $Q_d(s)$, which are represented in Fig. 2 are as follows:

$$Q_r(s) = F(s)G_{-}^{-1}(s) \tag{16}$$

$$Q_d(s) = \frac{1 + \alpha_1 s + \cdots + \alpha_m s^m}{(\lambda s + 1)^m} \tag{17}$$

To remove the effect of the disturbance dynamics $Q_d(s)$, it is necessary to fine-tune every aspect of the system, including the values of its parameters such as $\alpha_1, \ldots, \alpha_m$ and λ, in such a way that they are chosen properly. It is important to note that the acceptable range of the system's speed can be attained by selecting a suitable value for λ. Despite this, it is important to keep in mind that there is a trade-off that must be considered between the system speed and the controller efforts. For the purposes of this investigation, in accordance with the disturbances dynamics (according to the ρ and σ values in Assumption 1) a first-order low-pass filter with a large time constant $G_d(s) = \frac{1}{10s+1}$ as well as $\lambda = 0.05$ are considered in this study.

According to the $T_{dy}(s)$ transfer function, the ideal performance is when all of the input disturbances frequencies do not pass to the output, which represents the ratio between disturbances and output signals.

$$T_{dy}(s) = \frac{Y(s)}{D(s)} = (1 - Q_r Q_d(s)\tilde{G}(s))G_d(s) \tag{18}$$

The $Q_d(s)$ parameters have to be chosen in such a manner to mitigate all disturbance frequencies in the output signals as quickly as feasible. To accomplish this, the following condition needs to be satisfied:

$$T_{dy}(s)|_{\substack{s=-0.1 \\ \lambda=0.05}} = 0 \tag{19}$$

According to the $G_d(s)$ and $T_{dy}(s)$ transfer functions if the $Tdy(s)$ has a zero equal to the $G_d(s)$ pole at $s = -0.1$, the disturbance would be unable to reach the output $y(s)$, and thus the $G_d(s)$ dynamics are completely eliminated. In other words, the proposed IMC is utilized to improve the trade-off between set-point tracking and disturbance rejection in a good manner to keep both control goals within an acceptable range as defined by IEEE standards [30,31].

3.2. Proposed H_∞ robust control

H_∞ feedback controller in combination with a modified IMC control can enhance anti-disturbance capability as well as robustness in the face of unforeseen model uncertainties. Accordingly, system robustness can be guaranteed even in the presence of model uncertainties and external disturbance as well as measurement noises and time delay.

H_∞ control minimization is a control theory technique that enables the design of robust controllers for uncertain and complex systems. Its primary objective is to minimize the impact of external disturbances while maintaining specified performance levels. This technique achieves this goal by minimizing the H_∞ norm of the system transfer function, which represents the maximum gain from disturbance to output. H_∞ control is a powerful tool for control system design as it offers a systematic approach to developing robust controllers for complex systems, both continuous and discrete-time. It has several advantages, including

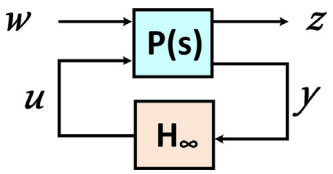

Fig. 3. The general configuration of the standard robust controller.

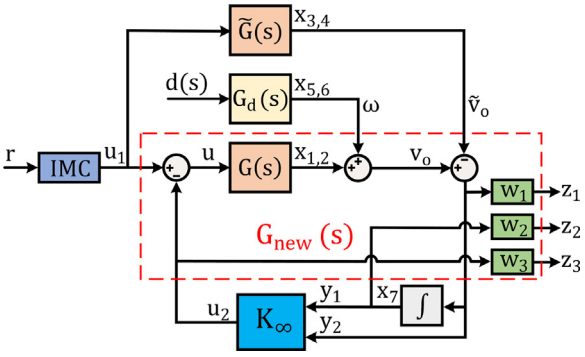

Fig. 4. The block diagram of the proposed H_∞ controller.

its ability to handle nonlinearities and uncertainties, incorporate design specifications, and apply to a wide range of applications.

Designing a H_∞ feedback controller using robust control theory provides system robustness when the controller is subject to model perturbations and external disturbances [32]. Compared to the conventional primary controller, the H_∞ internal model-based voltage controller can improve transient and steady-state performance and regulate output voltage more precisely.

The H_∞ feedback controller's design can be transferred as a standard robust control check. The H_∞ standard configuration in Fig. 3 provides the general formulation, as shown below.

$$\begin{bmatrix} z \\ y \end{bmatrix} = P(s) \begin{bmatrix} w \\ u \end{bmatrix} = \begin{bmatrix} P_{11}(s) & P_{12}(s) \\ P_{21}(s) & P_{22}(s) \end{bmatrix} \begin{bmatrix} w \\ u \end{bmatrix} \tag{20}$$

The following formulation yields $P(s)$:

$$P(s) = \begin{pmatrix} D_{11} & D_{12} \\ D_{21} & D_{22} \end{pmatrix} + \begin{pmatrix} C_1 \\ C_2 \end{pmatrix} (sI - A)^{-1} (B_1 B_2) \tag{21}$$

According to the standard robust control configuration, the $G_{new}(s)$ in this configuration can also be considered as the $P(s)$, as shown in Fig. 4. As can be seen, all of the components encircled by dashed lines can be viewed as $G_{new}(s)$ in order to consider the main problem as a standard robust control problem. The robust controller $K(s)$ is then utilized as a robust controller in a standard robust control problem. Where, u is the main control input, u_1 is the IMC output signal, u_2 is the H_∞ feedback controller output signal, $\tilde{V}_o$ is the estimated output voltage, ω is the external disturbance input signal, Z_i is the weighted performance output, W_i are the weighting factors. For the rest of the design procedures, $G_{new}(s)$ state-space model is needed. For this purpose, new state variables x_i, new inputs u_1 and u_2, new outputs z_i should be considered in order to drive the governing differential equations of the systems. Based on this, the state-space realization of the generalized plant $G_{new}(s)$ can be written as below.

$$G_{new,i}(s): \begin{cases} \dot{x} &= (A_i + \Delta A_i)x + (B_{1,i} + \Delta B_{1,i})w \\ &\quad +(B_{2,i} + \Delta B_{2,i})u \\ z_\infty &= (C_{1,i} + \Delta C_{1,i})x + (D_{11,i} + \Delta D_{11,i})w \\ &\quad +(D_{12,i} + \Delta D_{12,i})u \\ y &= (C_{2,i} + \Delta C_{2,i})x + (D_{21,i} + \Delta D_{21,i})w \\ &\quad +(D_{22,i} + \Delta D_{22,i})u \end{cases} \tag{22}$$

where, $x = [x_1, x_2, x_3, x_4, x_5, x_6, x_7]^T$, $z_\infty = [z_1, z_2, z_3]^T$, $y = [y_1, y_2]^T$, $w = [\omega, u_1]^T$ and $u = [u_2]$ are the states, control outputs, measured outputs disturbances and control input vectors, respectively. Moreover, A_i, $B_{1,i}$, $B_{2,i}$, $C_{1,i}$, $C_{2,i}$, $D_{11,i}$, $D_{12,i}$, $D_{21,i}$ and $D_{22,i}$ are the nominal system matrices and ΔA_i, $\Delta B_{1,i}$, $\Delta B_{2,i}$, $\Delta C_{1,i}$, $\Delta C_{2,i}$, $\Delta D_{11,i}$, $\Delta D_{12,i}$, $\Delta D_{21,i}$ and $\Delta D_{22,i}$ represent the model uncertainties for ith DGs.

Assumption 3. The model uncertainties ΔA_i, $\Delta B_{1,i}$, $\Delta B_{2,i}$, $\Delta C_{1,i}$, $\Delta C_{2,i}$, $\Delta D_{11,i}$, $\Delta D_{12,i}$, $\Delta D_{21,i}$, and $i \in \{1, 2, \ldots, N\}$, where N indicates the number of DG units, satisfies:

- $\left\| \Delta A_i^T \Delta A_i \right\|_\infty \leq 1$.
- $\left\| \Delta B_{1,i}^T \Delta B_{1,i} \right\|_\infty \leq 1$ and $\left\| \Delta B_{2,i}^T \Delta B_{2,i} \right\|_\infty \leq 1$.
- $\left\| \Delta C_{1,i}^T \Delta C_{1,i} \right\|_\infty \leq 1$ and $\left\| \Delta C_{2,i}^T \Delta C_{2,i} \right\|_\infty \leq 1$.
- $\left\| \Delta D_{11,i}^T \Delta D_{11,i} \right\|_\infty \leq 1$ and $\left\| \Delta D_{12,i}^T \Delta D_{12,i} \right\|_\infty \leq 1$.
- $\left\| \Delta D_{21,i}^T \Delta D_{21,i} \right\|_\infty \leq 1$ and $\left\| \Delta D_{22,i}^T \Delta D_{22,i} \right\|_\infty \leq 1$.

Where $\|\|_\infty$ is the infinity norm. All the nominal system matrices can be found in Appendix A.

Assumption 4. According to [33], following assumptions are made:

- (A, B_1) is stabilizable and (C_1, A) is detectable.
- (A, B_2) is stabilizable and (C_2, A) is detectable.
- $D_{12}^T \begin{bmatrix} C_1 & D_{12} \end{bmatrix} = \begin{bmatrix} 0 & I \end{bmatrix}$.

According to the controllability and observability concepts for a state space model of the system, the stabilizability and detectability concepts can be defined as follows:

- The stabilizability pertains to the property whereby all uncontrollable modes exhibit convergence.
- The detectability pertains to the property whereby all unobservable modes exhibit convergence.

For the sake of brevity, Appendix B contains all the calculations needed to prove the above assumptions.

The control law can be stated using the following formula, which is derived from the standard robust control problem:

$$u_2 = K(s)y \tag{23}$$

Then, the H_∞ control problem is to find the output feedback controller $K(s)$ which satisfies the following inequality:

$$\|T_{\omega \to z}(s)\|_\infty \triangleq \sup_{s=jw} \frac{\|z(s)\|_2}{\|w(s)\|_2} \leq \gamma \tag{24}$$

$$T_{\omega \to z}(s) = P_{11} + P_{12}K(I - P_{22}K)^{-1}P_{21} \tag{25}$$

where $T_{\omega \to z}(s)$ is the transfer function from the single input ω to multiple output z. This means that the H_∞ norm of $T_{\omega \to z}(s)$ is maintaining less than a prescribed value $\gamma > 0$. The procedure for selecting the weighting factors (W_i) in an $H\infty$ controller necessitates a balancing act between the desired characteristics of robustness and system performance. Weighting factors are employed to shape the closed-loop transfer function of the system and prioritize control objectives such as fast reference tracking, disturbance rejection, bounded control effort, etc. After making a number of trial-and-error selections for these weighting factors, these values were ultimately chosen as providing the best balance of robustness and performance ($W_1 = 30$, $W_2 = 20$ and $W_3 = 1$).

3.3. LMI formulation

In this section, the LMI formulation for calculating the controller $K(s)$ is discussed. The following is a lemma that can be used to turn the $H\infty$ constraints into an LMI, which ultimately results in obtaining the controller $K(s)$ parameters.

Lemma ([34]). *For a continuous-time transfer function $T_{\omega\to z}(s)$, the following statements are equivalent:*

- *The $\|T_{\omega\to z}(s)\|_\infty < \gamma$ and A is stable $R_e(\lambda_i(A)) < 0$.*
- *there exists a symmetric positive definite solution X to the below LMI:*

$$\begin{pmatrix} A^TX + XA & XB & C^T \\ B^TX & -\gamma I & D^T \\ C & D & -\gamma I \end{pmatrix} < 0 \tag{26}$$

Proof. See, e.g., [35], Page 82.

According to the [36], the following matrices should be considered to obtain the LMIs and in following to obtain the controller $K(s)$ parameters as below:

$$\begin{cases} H_{X_{cl}} = \begin{bmatrix} \bar{A}_\infty^T X_{cl} + X_{cl}\bar{A}_\infty & X_{cl}\bar{B}_\infty & \bar{C}_\infty^T \\ \bar{B}_\infty^T X_{cl} & -\gamma I & D_{11}^T \\ \bar{C}_\infty & D_{11} & -\gamma I \end{bmatrix} \\ P_{X_{cl}} = \begin{bmatrix} \underline{B}_\infty^T X_{cl} & 0 & \underline{D}_{12\infty}^T \end{bmatrix} \\ Q_\infty = \begin{bmatrix} \underline{C}_{1\infty} & \underline{D}_{21\infty} & 0 \end{bmatrix} \end{cases} \tag{27}$$

where

$$X_d = \sqrt{X - Y^{-1}} \quad X_{cl} = \begin{bmatrix} X & X_d \\ X_d^T & I \end{bmatrix} \quad \bar{A}_\infty = \begin{bmatrix} A & 0 \\ 0 & 0 \end{bmatrix}$$

$$\underline{B}_\infty = \begin{bmatrix} 0 & B_2 \\ I & 0 \end{bmatrix} \quad \bar{C}_{1\infty} = \begin{bmatrix} C_1 & 0 \end{bmatrix} \quad \bar{B}_\infty = \begin{bmatrix} B_1 \\ 0 \end{bmatrix}$$

$$\underline{C}_{1\infty} = \begin{bmatrix} 0 & I \\ C_3 & 0 \end{bmatrix} \quad \underline{D}_{12\infty} = \begin{bmatrix} 0 & D_{12} \end{bmatrix} \quad \underline{D}_{21\infty} = \begin{bmatrix} 0 \\ D_{21} \end{bmatrix}$$

Finally, the controller parameters K_∞ are obtained by solving the following LMI condition with the MATLAB LMI toolbox:

$$H_{X_{cl}} + Q_\infty^T K_\infty^T P_{X_{cl}} + P_{X_{cl}}^T K_\infty Q_\infty < 0 \tag{28}$$

where

$$K_\infty = \begin{bmatrix} A_{k\infty} & B_{k\infty} \\ C_{k\infty} & D_{k\infty} \end{bmatrix} \tag{29}$$

For the sake of brevity, Appendix C lists all of the controller parameters K_∞ only for DG 1. A more in-depth discussion of the LMI design procedure can be found in [37].

3.4. Voltage control of DC microgrids with boost converters

The main model presented in the DCMG modeling section can accommodate various types of DC–DC converters, as mentioned earlier. In the DCMG system described here, the DG_k is typically a DC–DC boost converter. Fig. 2a depicts the updated DCMG configuration. The following mathematical expression describes the DG_k with N_i neighbors:

$$\text{DG}\,k: \begin{cases} \frac{dV_k}{dt} = \frac{D_k}{C_k} I_k - \frac{1}{C_k} I_{L_k} + \frac{1}{C_k} \sum_{j\in N_i} \frac{V_j - V_k}{R_{kj}} \\ \frac{dI_k}{dt} = -\frac{D_k}{L_k} V_k - \frac{R_k}{L_k} I_k + \frac{1}{L_k} V_{dc_k} \end{cases} \tag{30}$$

where $D_k = 1 - d_{boost_k}$ and d_{boost_k} is the duty cycle of the DC–DC boost converter of the DG_k. It should be mentioned that the new system configuration with a DC–DC boost converter results in a nonlinear system, unlike the previous configuration with DC–DC buck converters. This is because two nonlinear terms, D_kV_k and D_kI_k, are now present in the system. However, the control schemes presented in this study incorporate the nominal model of the system, which eliminates the need for linearization before applying the controller. This approach accounts for nonlinearities during the controller design process, assuming that the nominal model ($\tilde{G}(s)$) is sufficiently close to the actual system ($G(s)$). Ideally, an IMC controller could be designed if $G(s)$ and its inverse model were perfect, as mentioned in Assumption 2. However, it is difficult to achieve the inverse model in practice due to the presence of inertial and integration elements in the process. To ensure robustness against modeling mismatches and stability in the presence of differences between $\tilde{G}(s)$ and $G(s)$, a filter like $F(s)$ is required. As mentioned earlier, the proposed method does not require linearization if an accurate model of the system is used. In other words, the controller design procedures for the DCMG with nonlinear converters are the same as those for the DCMG with linear converters.

Table 1
Specification of the testbed DCMG.

DG #	DC–DC Buck Converter Parameters			Load (Ω)	Voltage reference
	R_t(Ω)	L_t (mH)	C_t (mF)		(V)
1	0.2	1.8	2.2	9	47.9
2	0.2	2.0	2.1	7	48.0
3	0.3	2.0	1.9	18	47.7
4	0.1	1.8	1.8	4	48.0
5	0.6	2.8	2.2	6	47.8
6	0.2	1.8	2.1	7	48.1

Table 2
Distribution network parameters.

Line Impedance Z_{ij}	R_{ij}(Ω)	L_{ij}(mH)
Z_{12}	0.05	1.8
Z_{13}	0.06	1.7
Z_{34}	0.07	1.7
Z_{24}	0.08	1.8
Z_{45}	0.07	1.8
Z_{16}	0.06	1.5
Z_{56}	0.05	1.3

4. Simulation results

To evaluate the proposed methodology in this study, a model of an islanded DCMG consisting of 6 DGs with buck converters is used. This model, which is based on [18], is shown in Fig. 5 and serves as an example of a conventional method for controlling DCMG voltage. The method that is suggested is an offline decentralized control scheme for the purpose of ensuring that the voltage stability in DCMG is maintained. This method has the potential to have a general interconnection topology, PnP functionalities, and the capacity to be scaled up for a large network. Tables 1 and 2 summarize the parameters of DGs and the distribution network, respectively. It is important to note that to demonstrate the effectiveness of the proposed method, some modifications are applied to distribution line characteristics and loads based on the parameters provided in [18]. Note also that white noise is added to the outputs of each DG unit to simulate an external disturbance. A variety of case studies is also considered to investigate how well the proposed RIMVC scheme performs in terms of voltage tracking ability, PnP functionality, and robustness to load changes and parameter variations. These include voltage tracking, load changing, PnP functionalities, robustness evaluation for parameter fluctuations in transient and steady-state performance, and in the presence of CPLs, and internal system delay following IEEE standards [31], which are discussed below.

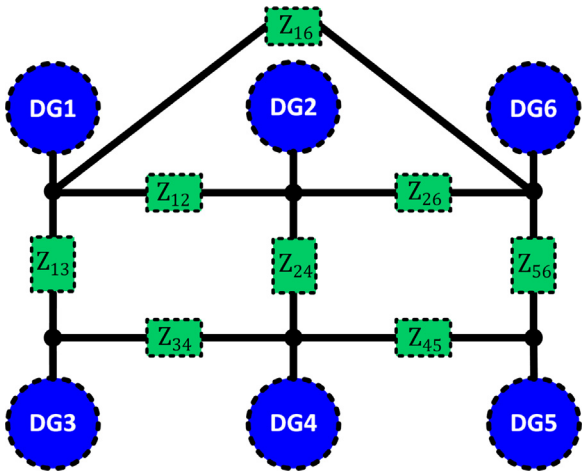

Fig. 5. Islanded DCMG consisting of 6 DGs as case study.

4.1. Case study 1: Voltage tracking

In this case study, the proposed control scheme is evaluated and compared with the conventional voltage control presented in [18] regarding the reference tracking quality in DG 1 and DG 3 simultaneously. The dynamic response of the DGs output voltages, the dynamic error between the set points and output voltages and control efforts are depicted in Fig. 6. As shown in Fig. 6, both the proposed and conventional controllers enables DGs to quickly track the variations of the reference voltage in their output with an acceptable error range. The difference is that the proposed RIMVC offers a lower voltage tracking error and demands a lower energy cost (i.e., a lower control effort).

4.2. Case study 2: Load change

A key requirement of voltage control schemes is the ability to maintain an acceptable output voltage deviation while loads vary. The dynamic output voltage and current of all DGs with both the proposed IMVC and the conventional voltage control under severe load changes (up to 40% of nominal loads) are shown in Fig. 7 and Fig. 8, respectively. It is observed that the proposed control strategy is still within acceptable output voltage deviations (according to the abovementioned IEEE standard [31]). The proposed RIMCV performs better in transient and steady-state responses, as demonstrated.

4.3. Case study 3: PnP functionality

In this case study, the proposed control scheme's PnP functionality is compared to the conventional voltage controller in [18]. To do so, we physically disconnect DG 5 from the main network at t = 2 s, and reconnect it at t = 4 s (as shown in Fig. 10), causing changes to the network structure that directly or indirectly affect DGs connected to DG 5. To ensure a fair comparison, a bumpless transfer scheme is used. This scheme avoids unexpected shifts in the controller variables and provides a smooth transition during plug-out and plug-in switching times. The bumpless transfer scheme procedure, which was first studied for manually switching between different PIDs, is discussed in more detail in [38]. Fig. 9 highlights that the DGs connected to DG 5 perform better with the proposed control scheme in terms of voltage regulation. The DCMG system is shown to be robust, and the PnP functionality of DG5 has no impact on the system's stability. Therefore, no changes are necessary to the local controller's operation.

4.4. Case study 4: Robustness for parameters fluctuation

The robustness of the proposed control scheme in the presence of parameter uncertainties is evaluated in this section. Since the DC–DC converter parameters (such as C_i, L_i and R_i) fluctuate more frequently in practice than other parameters, the robustness analysis is investigated in terms of uncertainty in these parameters. According to the IEEE standards [31], a device connected to a 48 V rural DCMG system can have a normal operation and still be stable in terms of transient performance (for a short time) if the system provides voltage in the range of 36 to 58. As shown in Fig. 11, with RIMCV in DG1, the system remains stable by adding 40% variation to all of the abovementioned DC–DC converter parameters. However, the conventional controller cannot handle this situation, leading to instability. This observation confirms the superiority of the proposed controller in terms of robustness to uncertainties compared to the conventional controller.

4.5. Case study 5: Robustness evaluation in presence of CPLs and internal disturbances

In this case study, the robustness of the proposed method is evaluated in the presence of the different constant power loads (CPLs). To this end, six CPLs with different capacities are considered as the local loads according to the DCMG configuration in this paper, as depicted in Fig. 5. It should be noted that, as we considered the $u_i = d_{buck_i} V_{dc_i}$ as the control signal for the IMC controller, any changes to the input voltage source (V_{dc_i}) can be considered as internal disturbances. These internal disturbances are added to the generated control signal by the IMCs and lead further away from the desired control goals of the IMCs, such as the appropriate fast reference tracking in the presence of external disturbances in the measured output. Therefore, another control loop is needed to keep the system performance within the acceptable range even in the presence of internal disturbances not considered in the IMC design procedure and not covered by the IMC. In the proposed RIMVC methods, the H_∞ controller is added to the inner IMC loop to improve the system performance not only in the presence of the model parameter uncertainties but also in the un-modeled internal disturbances. As you can see in Figs. 12 and 13, in case study 5, although the system has six different times varied input voltage source profiles, the CPLs have absorbed the constant power from the network even in the presence of unmodeled internal disturbances and reference changes in two different DGs (DG 1 and DG 3) which shown the effectiveness and the robustness of the proposed method. Moreover, it should be mentioned that the final control effort signals (U) for the rest of the DG units, which do not have any reference changes (DG 2, DG 4, DG 5, and DG6), remain constant even the internal disturbances are injected to the plant. In other words, the H_∞ controller (U2) tries to compensate for the negative consequences of the injected internal disturbances (time-varying input voltage source (V_{dc_i}), which are manipulated by the IMC control signals (U1). Moreover, the final control effort signal (U) for the units that have reference changes is not constant and has changed to make the appropriate response to the input reference changes.

4.6. Case study 6: Utilizing different types of DC-DC converters

This case study demonstrates the versatility of the proposed RIMVC control scheme by testing it on a DCMG system that employs two different DC–DC boost converters, DG1 and DG2. The study aims to show that the proposed control scheme is not limited to DCMGs with linear converters such as buck converters,

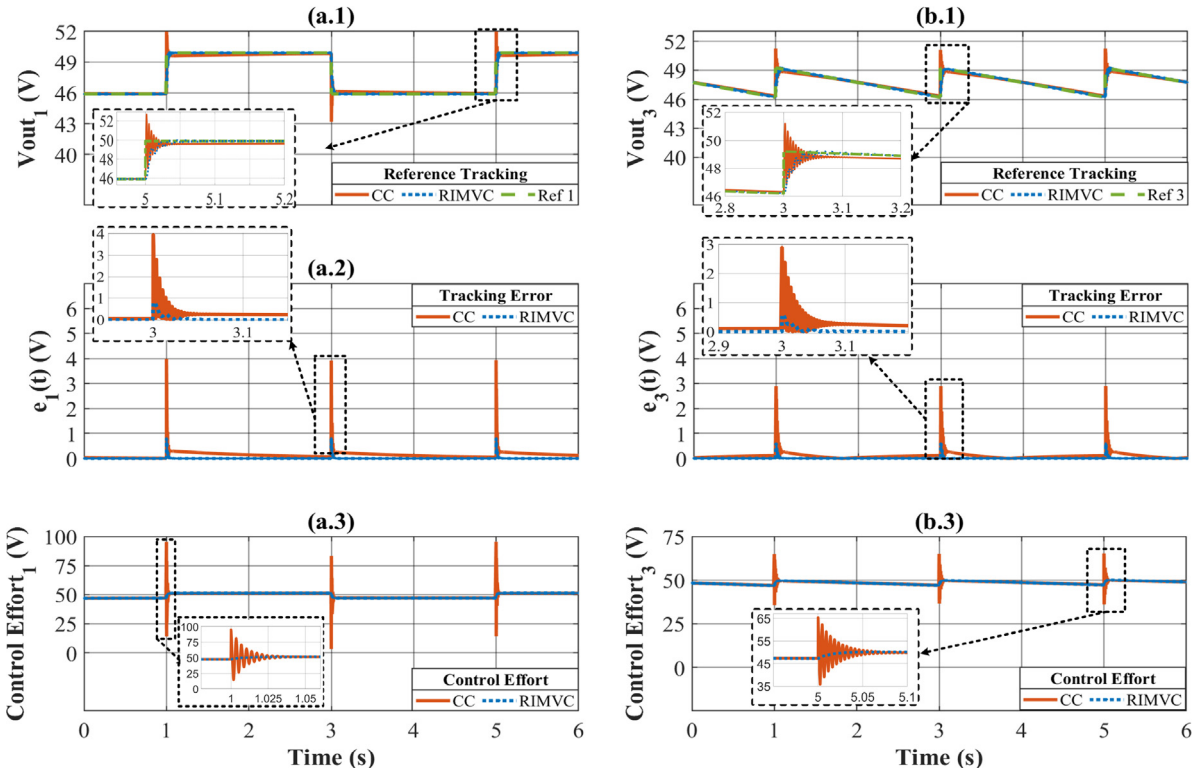

Fig. 6. Performance evaluation of the DG 1 and DG 3, with respect to voltage reference variations: (a.1) Output voltage of DG 1, (a.2) Voltage tracking error of DG 1, (a.3) Controller effort of DG 1, (b.1) Output voltage of DG 3, (b.2) Voltage tracking error of DG 3, (b.3) Controller effort of DG 3.

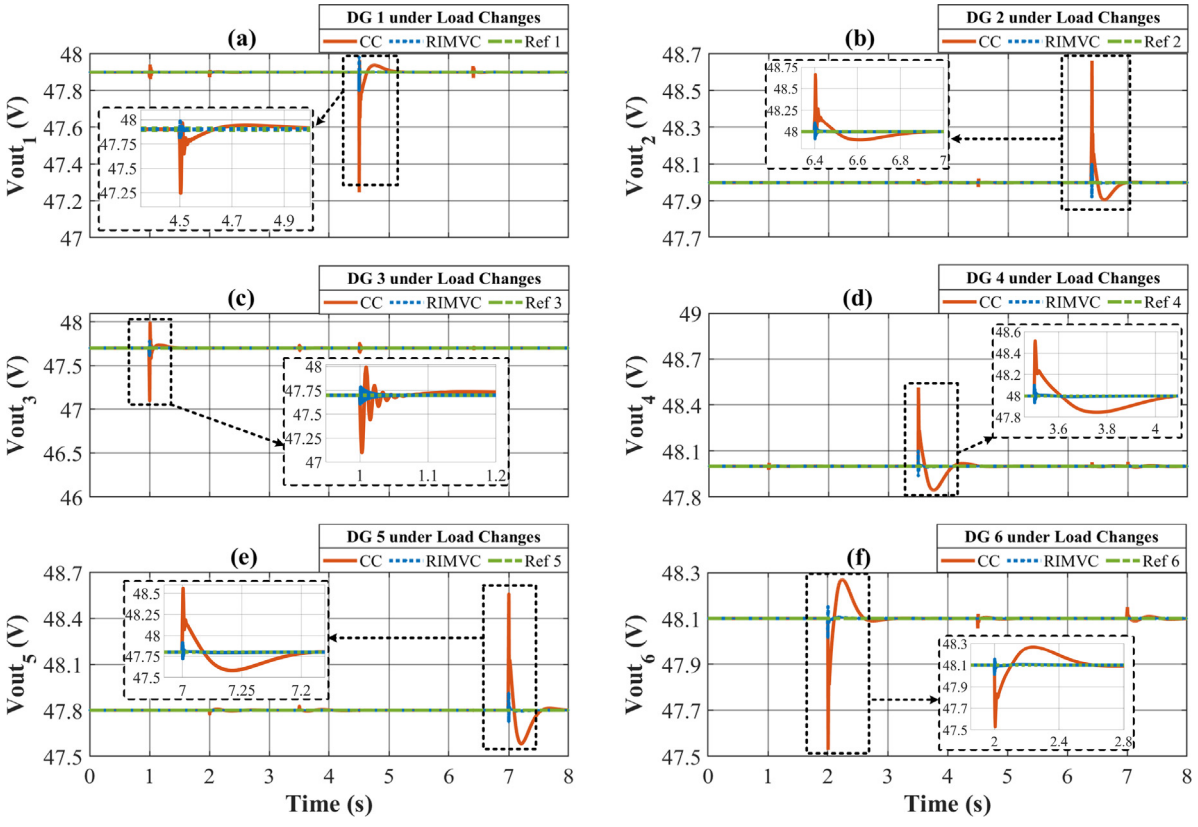

Fig. 7. Output voltages of all DGs under load variations: (a) DG 1, (b) DG 2, (c) DG 3, (d) DG 4, (e) DG 5, (f) DG 6.

but can also be applied to systems with different types of converters that may introduce nonlinearities into the system model.

To evaluate the performance of the DCMG system under different types of DC–DC converters and in the presence of internal

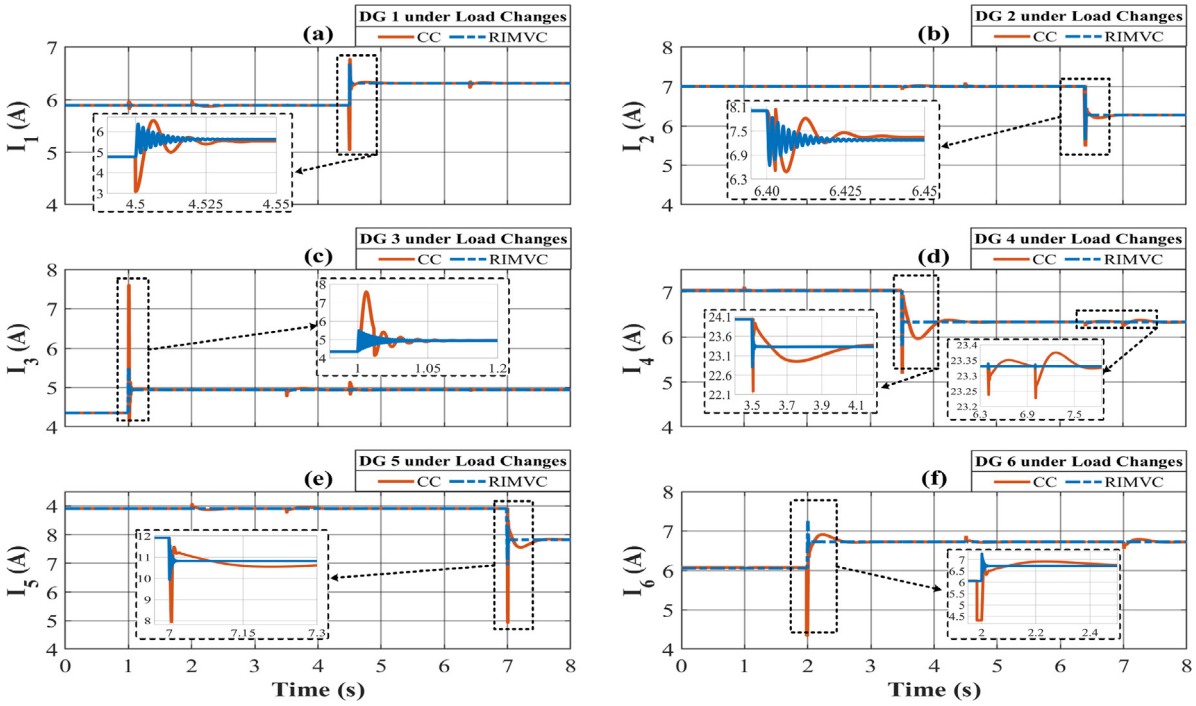

Fig. 8. Output currents of all DGs under load variations: (a) DG 1, (b) DG 2, (c) DG 3, (d) DG 4, (e) DG 5, (f) DG 6.

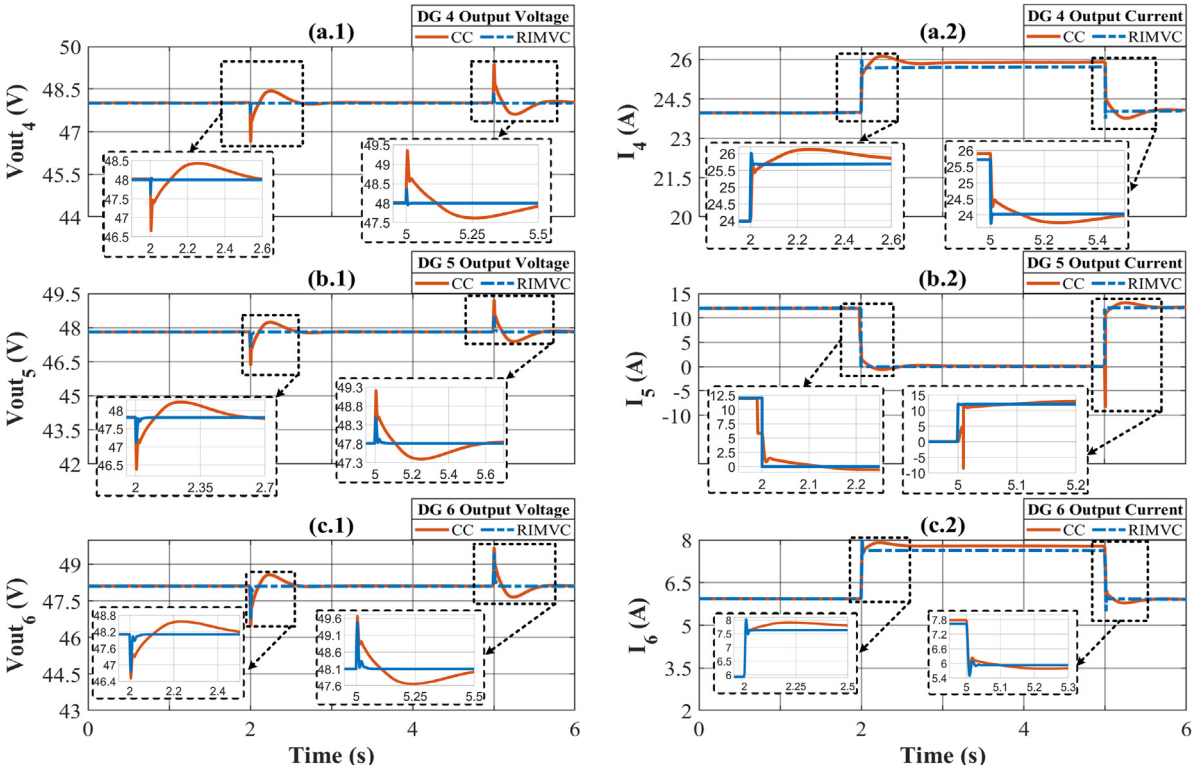

Fig. 9. PnP functionality evaluation of DGs: (a) Output Voltage DG 4, (b) Output Current DG 4, (c) Output Voltage DG 5, (d) Output Current DG 5, (e) Output Voltage DG 6, (f) Output Current DG 6.

disturbances caused by time-varying voltage sources, the voltage tracking scenario from Case Study 2 is repeated. The results, as presented in Figs. 14 and 15, show that the proposed RIMVC technique maintains acceptable system performance even when various DC–DC converters are used.

4.7. Case study 7: System delay and external disturbances

In this case study, the system performance is evaluated by considering the proposed method in the presence of a large system delay of 1 s (e^{-s}) and external disturbances simultaneously, for two units (DG 1 and DG 5). As discussed earlier in Section 3.1, in

Table 3
Performance comparison between the proposed method and the conventional control.

Controller type	Scenarios			
RIMVC	Case Study 1	Case Study 2	Case Study 3	Case Study 4
	DG1 → IAE = 0.79, $\|u\|_2$ = 189.9 DG3 → IAE = 1.47, $\|u\|_2$ = 187.8	DG1 → IAE = 0.87, $\|u\|_2$ = 178.4 DG2 → IAE = 1.03, $\|u\|_2$ = 179.8 DG3 → IAE = 1.17, $\|u\|_2$ = 181.1	DG4 → IAE = 1.08, $\|u\|_2$ = 164.3 DG5 → IAE = 1.19, $\|u\|_2$ = 153.2 DG6 → IAE = 1.63, $\|u\|_2$ = 181.1	DG1 → IAE = 0.67, $\|u\|_2$ = 213.2 DG2 → IAE = 0.41, $\|u\|_2$ = 196.5 DG3 → IAE = 0.84, $\|u\|_2$ = 187.6
	Case Study 5		Case Study 6	Case Study 7
	DG1 → IAE = 7.597, $\|u\|_2$ = 189.2 DG2 → IAE = 5.604, $\|u\|_2$ = 195.4 DG3 → IAE = 7.406, $\|u\|_2$ = 185.6	DG4 → IAE = 10.45, $\|u\|_2$ = 215.1 DG5 → IAE = 8.063, $\|u\|_2$ = 205.8 DG6 → IAE = 7.062, $\|u\|_2$ = 200.4	DG1 → IAE = 1.03, $\|u\|_2$ = 189.9 DG3 → IAE = 5.646, $\|u\|_2$ = 187.5 DG5 → IAE = 2.256, $\|u\|_2$ = 205.5	DG1 → IAE = 8.535, $\|u\|_2$ = 218.1 DG5 → IAE = 10.06, $\|u\|_2$ = 231.9
CC	Case Study 1	Case Study 2	Case Study 3	Case Study 4
	DG1 → IAE = 6.42, $\|u\|_2$ = 199.9 DG3 → IAE = 6.21, $\|u\|_2$ = 198.7	DG1 → IAE = 4.65, $\|u\|_2$ = 189.6 DG2 → IAE = 5.43, $\|u\|_2$ = 195.3 DG3 → IAE = 5.26, $\|u\|_2$ = 186.1	DG4 → IAE = 5.85, $\|u\|_2$ = 200.3 DG5 → IAE = 4.37, $\|u\|_2$ = 187.2 DG6 → IAE = 4.61, $\|u\|_2$ = 233.1	DG1 → IAE = NotApplicable, $\|u\|_2$ = NotApplicable DG2 → IAE = NotApplicable, $\|u\|_2$ = NotApplicable DG3 → IAE = NotApplicable, $\|u\|_2$ = NotApplicable
	Case Study 5, 6, 7			
	Not Applicable			

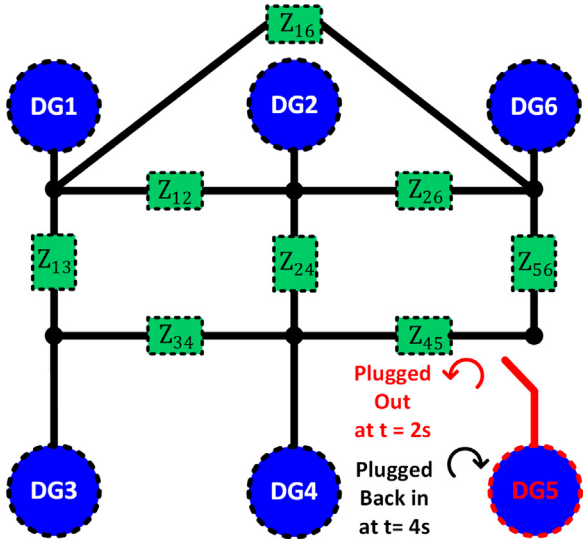

Fig. 10. Layout of the understudy DCMG following a topology change to evaluate the DG 5's PnP functionality.

the presence of any time delay in the system, the modified IMC controller is responsible for generating an appropriate control signal for providing acceptable system performances according to the desired control goals. It should be mentioned that as the time delay belongs to the group of NMP terms (Eq. (8)), by considering the pade approximation (Eq. (10)), the updated model transfer function for instance for DG 5 could also be reformulated as follows:

$$G_{5+}(s) = e^{-s} \tag{31}$$

$$G_{5-}(s) = G_5(s)G_{5+}^{-1}(s) \tag{32}$$

$$\tilde{G}_5(s) = G_5(s)\left(\frac{1-\frac{1}{2}s}{1+\frac{1}{2}s}\right) \tag{33}$$

Moreover, in the presence of external large-signal disturbances as depicted in Fig. 16(a.4) and (b.4), both IMC and H_∞ controllers are operated to attenuate the negative consequence of the disturbances Fig. 16(a.3) and (b.3). It is worth mentioning that as soon as any changes occur in the reference' signals, although the system equations have an internal time delay, the IMC controller (U1) start to react to changes while the effect of this reaction will effect on the future of the system. In other words, by utilizing this control technique, the time delay will be removed from the control loop to the output side of the system. Therefore, although the controller reacts to the reference changes at t=1, the system output will change after 1 s time delay at t=2, as depicted in Fig. 16(a.1) and (b.1).

5. Discussion

In this section, two quantitative measures, i.e., Integral Absolute Error (IAE) and 2-norm of the control effort, are used to more precisely evaluate the proposed control and conventional control schemes for the considered DCMG. The calculation formulas for these indices are as follows:

$$IAE := \int_0^\infty (r(t)_i - y(t)_i)dt \tag{34}$$

$$\|u\|_2 := \left(\int_{-\infty}^{\infty} u(t)^2 dt\right)^{\frac{1}{2}} \tag{35}$$

Table 3 presents a comprehensive performance analysis of the proposed RIMVC control scheme and the conventional control system in terms of Integral of Absolute Error (IAE) and 2-norm of control effort for each DG unit. The results show that the RIMVC outperforms the conventional control in all simulation scenarios. In scenarios 1–3, the RIMVC achieves lower IAE for voltage tracking while using less control effort (energy) than the conventional control system. In scenarios 4–7, the robustness of the RIMVC is demonstrated in the presence of model parameter uncertainties, CPLs, internal and external disturbances, different types of DC–DC converters, and system time delay. Conversely, the conventional control system exhibits instability in these scenarios, and the performance indices values are not applicable.

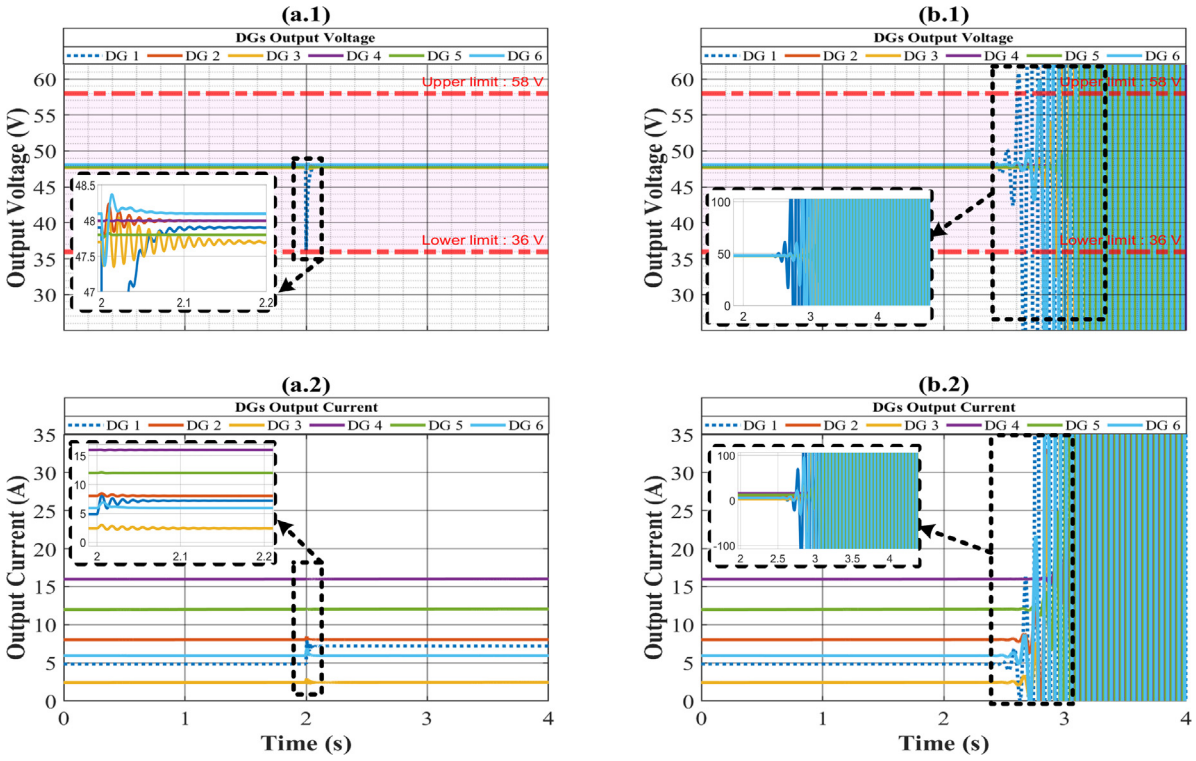

Fig. 11. Performance comparison of the proposed RIMVC, in the presence of model uncertainties for the DC–DC converter parameters in DG 1: (a.1) DGs output voltage with RIMVC, (a.2) DGs output current with RIMVC, (b.1) DGs output voltage with conventional control, (b.2) DGs output current with conventional control.

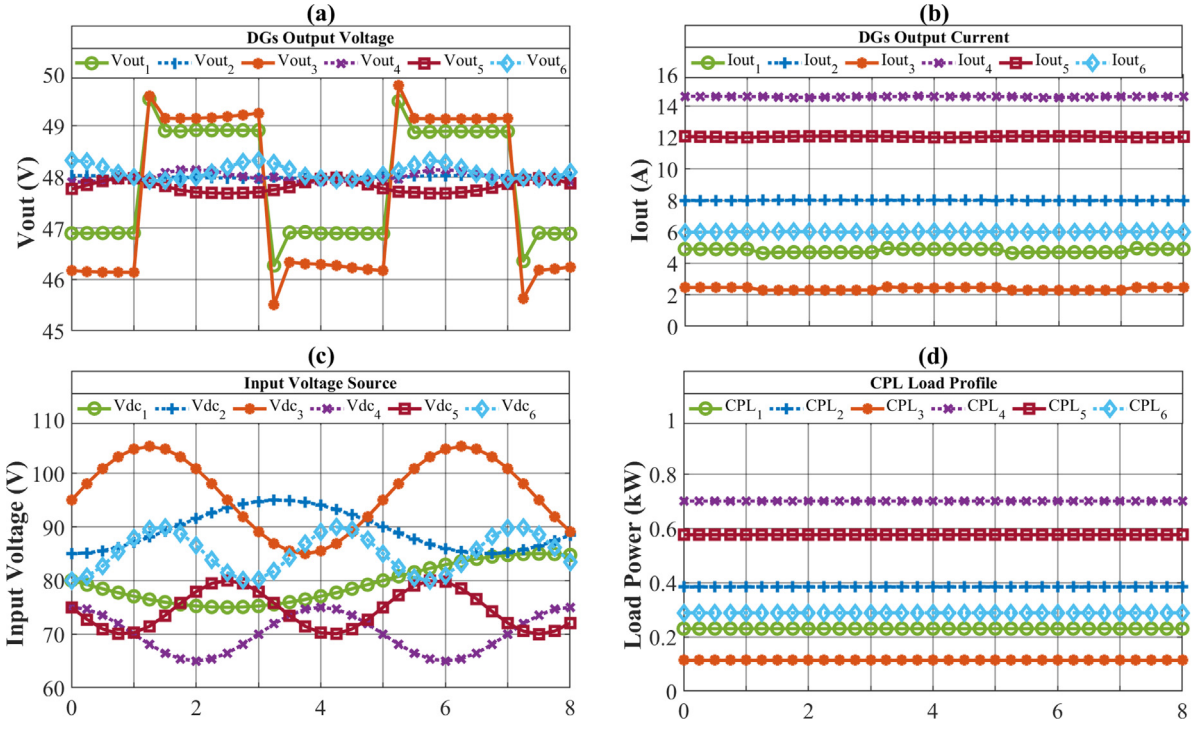

Fig. 12. Performance comparison of the proposed RIMVC with CPLs, in the presence of model uncertainties for all DGs: (a) DGs output voltage with RIMVC, (b) DGs output current with RIMVC, (c) DGs input voltage source, (d) Load Profile (CPLs).

6. Conclusion

This paper proposes a modified robust IMC-based control scheme as a voltage control strategy for DCMGs. The performance of the proposed method was validated using real-time simulations in the MATLAB/Simulink environment to assess its efficiency and accuracy under multiple scenarios. The results demonstrate that the proposed controller can maintain reference voltage tracking in the presence of unknown external disturbances; for the sake of comprehensivity, white noises are used

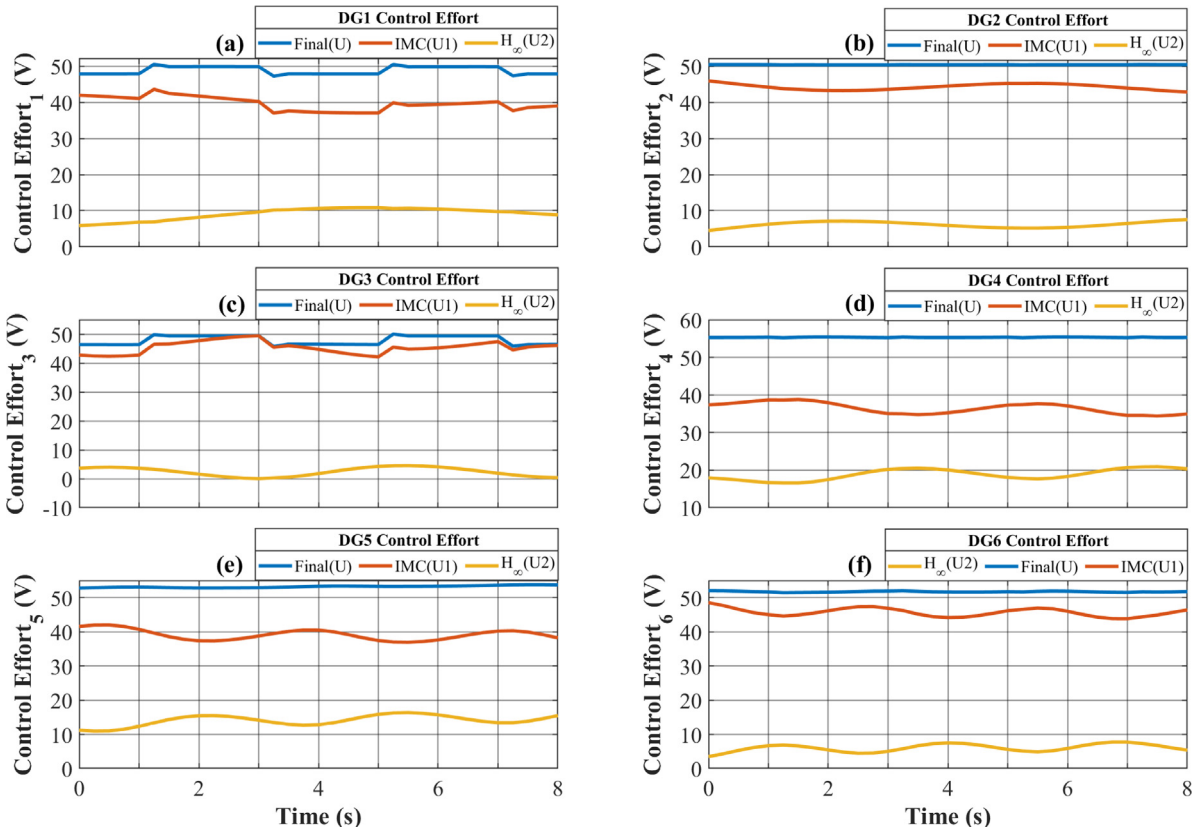

Fig. 13. Control effort signal of all DGs: (a) DG 1, (b) DG 2, (c) DG 3, (d) DG 4, (e) DG 5, (f) DG 6.

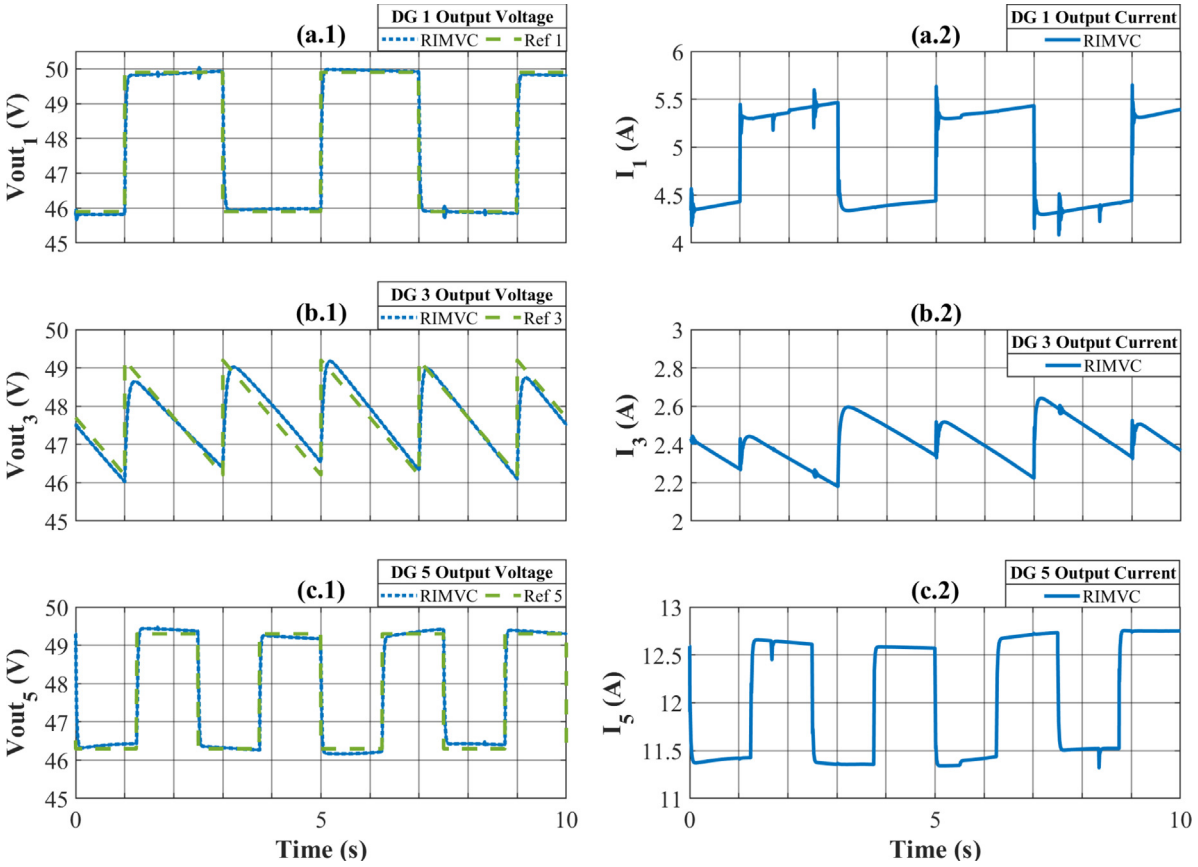

Fig. 14. Performance evaluation of DCMG system with DC–DC boost converters in DG 3 and DG 5: (a.1) Output Voltage DG 1, (a.2) Output Current DG 1, (b.1) Output Voltage DG 3, (b.2) Output Current DG 3, (c.1) Output Voltage DG 5, (c.2) Output Current DG 5.

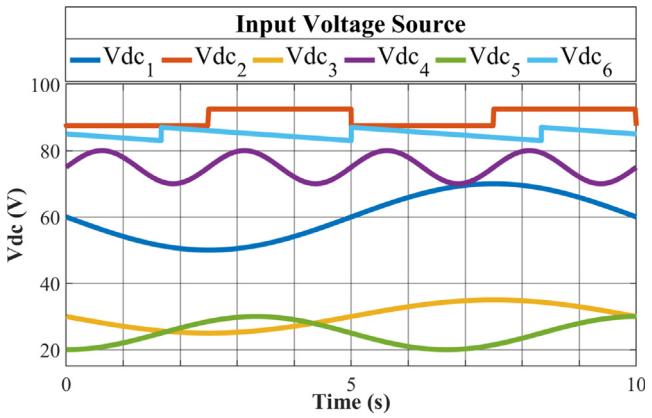

Fig. 15. Input voltage sources of all DGs: (a) DG 1, (b) DG 2, (c) DG 3, (d) DG 4, (e) DG 5, (f) DG 6.

in this study, while the system is evaluated in terms of having a wide range of load and voltage reference changes, model parameter uncertainties, as well as the unit PnP functionalities. In conclusion, the RIMVC responded better than other conventional voltage control schemes due to its ability to remove external disturbances and measurement noise in the presence of model uncertainties. RIMVC significantly reduces output voltage peaks, transient response, and settling time when unknown external disturbances are injected into the measured data. Some of the good achievements that were confirmed through the simulation results include a fast-tracking response and a bounded control effort. Extending the proposed method by adding other types of converters and relaxing some of the considered assumptions in this paper are the subject of future studies by the authors.

CRediT authorship contribution statement

Amir Basati: Conceptualization, Methodology, Investigation, Resources, Software, Data curation, Visualization, Formal analysis, Writing – original draft, Writing – review & editing. **Josep M. Guerrero:** Supervision, Writing – review & editing. **Juan C. Vasquez:** Supervision, Writing – review & editing. **Ahmad Fakharian:** Supervision, Writing – review & editing. **Karl Henrik Johansson:** Supervision, Writing – review & editing. **Saeed Golestan:** Writing – review & editing.

Declaration of competing interest

The authors declare that they have no known competing financial interests or personal relationships that could have appeared to influence the work reported in this paper.

Data availability

No data was used for the research described in the article.

Acknowledgments

This work was supported by VILLUM FONDEN, Denmark, under the VILLUM Investigator Grant (no. 25920); Center for Research on Microgrids (CROM), http://www.crom.et.aau.dk.

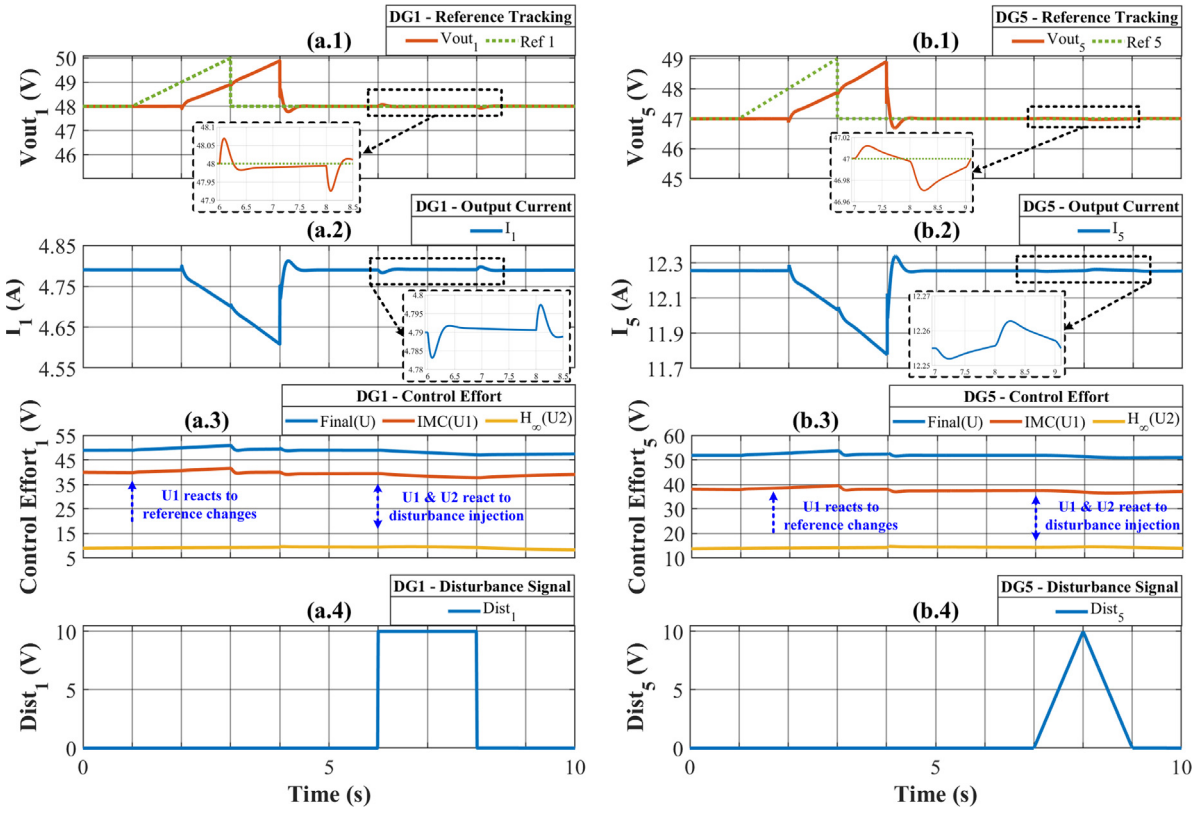

Fig. 16. Performance evaluation of the DG 1 and DG 5, with respect to 1 s time delay and voltage reference variations: (a.1) Output voltage of DG 1, (a.2) Output Current of DG 1, (a.3) Controller effort of DG 1, (a.4) External Disturbance Injection into DG 1, (b.1) Output voltage of DG 5, (b.2) Output Current of DG 5, (b.3) Controller effort of DG 5, (b.4) External Disturbance Injection into DG 5.

Appendix A

Since the parameters of each DG unit differ slightly, all of the system matrices A, B_1, B_2, C_1, C_2, D_{11}, D_{12}, D_{21} and D_{22} for all DG units are almost similar. For instance, all of the system matrices for $DG1$ are only listed below. **DG1:**

$$A=\begin{bmatrix} 0 & 1 & 0 & 0 & 0 & 0 & 0 \\ -2.60\times10^5 & -179.3 & 0 & 0 & 0 & 0 & 0 \\ 0 & 0 & 0 & 1 & 0 & 0 & 0 \\ 0 & 0 & -2.60\times10^5 & -179.3 & 0 & 0 & 0 \\ 0 & 0 & 0 & 0 & 0 & 1 & 0 \\ 0 & 0 & 0 & 0 & -100 & -20 & 0 \\ 1 & 0 & -1 & 0 & 1 & 0 & 0 \end{bmatrix} C_1=\begin{bmatrix} 30 & 0 & -30 & 0 & 30 & 0 & 0 \\ 0 & 0 & 0 & 0 & 0 & 0 & 20 \\ 0 & 0 & 0 & 0 & 0 & 0 & 0 \end{bmatrix} D_{22}=\begin{bmatrix} 0 \\ 0 \end{bmatrix}$$

$$B_1=\begin{bmatrix} 0 & 0 \\ 0 & 2.52\times10^5 \\ 0 & 0 \\ 0 & 2.52\times10^5 \\ 0 & 0 \\ 1 & 0 \\ 0 & 0 \end{bmatrix} B_2=\begin{bmatrix} 0 \\ 2.52\times10^5 \\ 0 \\ 0 \\ 0 \\ 0 \\ 0 \end{bmatrix} C_2=\begin{bmatrix} 1 & 0 & -1 & 0 & 1 & 0 & 0 \\ 0 & 0 & 0 & 0 & 0 & 0 & 1 \end{bmatrix} D_{11}=\begin{bmatrix} 0 & 0 \\ 0 & 0 \\ 0 & 0 \end{bmatrix} D_{12}=\begin{bmatrix} 0 \\ 0 \\ 1 \end{bmatrix} D_{21}=\begin{bmatrix} 0 & 0 \\ 0 & 0 \end{bmatrix}$$

Appendix B

Stabilizability Check: To check if the pair (A, B_1) is stabilizable, the following steps should be performed:
(I) Firstly, We need to compute the controllability matrix of the system defined by (A, B_1), which is given by:

$$Co=\begin{bmatrix} B_1 & A*B_1 & A^2*B_1 & \cdots & A^{n-1}*B_1 \end{bmatrix} \tag{B.1}$$

where n = 7 is the order of matrix A which is a 7-by-7 matrix.
(II) Secondly, we need to check the rank of the controllability matrix. If the rank of Co matrix is equal to the n, then the pair (A, B_1) is said to be controllable. If the rank of Co is less than n, then we need to use for instance the Kalman decomposition to decompose the system into controllable and uncontrollable subsystems. $Rank(Co) = 3 < 7$, therefore we need to check if all these four uncontrollable states are stabilizable or not. The controllable subsystem is given by:

$$A_c=T^{-1}AT=1.0\times10^5*\begin{bmatrix} 0.0025 & -0.0000 & -0.0000 & -0.0000 & -0.0000 & 0 & 0 \\ 2.6010 & -0.0043 & -0.0000 & -0.0000 & -0.0000 & 0 & 0 \\ 0.0000 & -0.0000 & -0.0000 & -0.0000 & 0.0000 & 0 & 0.0000 \\ -0.0000 & 0.0000 & 0.0000 & 0.0000 & 0 & 0 & -0.0000 \\ 0 & 0 & 0 & 0 & 0 & -0.0000 & 0 \\ 0 & 0 & 0 & 0 & 0.0010 & -0.0002 & 0 \\ 0.0000 & 0.0000 & -0.0000 & 2.6010 & 0 & 0 & -0.0018 \end{bmatrix} \tag{B.2}$$

where T is a controllability transformation matrix.
(III) Then, we need to check the eigenvalues of the controllable subsystem A_c. If all the eigenvalues of A_c have negative real parts, then the controllable subsystem is stable and the pair (A, B1) is stabilizable. If any eigenvalue of A_c has a positive real part, then the controllable subsystem is unstable and the pair (A, B1) cannot be stabilized by any feedback control law.

$$eig(A_c)=1.0\times10^2*\begin{bmatrix} -0.0000+0.0000i \\ -0.8965+5.0206i \\ -0.8965-5.0206i \\ -0.8965+5.0206i \\ -0.8965-5.0206i \\ -0.1000+0.0000i \\ -0.1000+0.0000i \end{bmatrix} \tag{B.3}$$

Therefore, due to all the eigenvalues of A_c having negative real parts, then the controllable subsystem is stable and the pair (A, B_1) is stabilizable. To check if the pair (A, B_2) is stabilizable, we should follow the abovementioned steps, therefore, we have: $Rank(Co) = 2 < 7$, therefore we need to check if all these five uncontrollable states are stabilizable or not.

$$A_c=T^{-1}AT=1.0\times10^5*\begin{bmatrix} -0.0002 & -0.0010 & 0 & 0 & 0 & 0 & 0 \\ 0.0000 & 0 & 0 & 0 & 0 & 0 & 0 \\ 0 & 0 & -0.0018 & -2.6010 & 0 & 0 & 0 \\ 0 & 0 & 0.0000 & 0 & 0 & 0 & 0 \\ 0 & 0.0000 & 0 & -0.0000 & 0 & 0.0000 & 0 \\ 0 & 0 & 0 & 0 & 0 & 0 & 0.0000 \\ 0 & 0 & 0 & 0 & 0 & -2.6010 & -0.0018 \end{bmatrix} \tag{B.4}$$

$$eig(A_c) = 1.0 \times 10^2 * \begin{bmatrix} -0.0000 + 0.0000i \\ -0.1000 + 0.0000i \\ -0.1000 + 0.0000i \\ -0.8965 + 5.0206i \\ -0.8965 - 5.0206i \\ -0.8965 + 5.0206i \\ -0.8965 - 5.0206i \end{bmatrix} \tag{B.5}$$

Therefore, due to all the eigenvalues of A_c having negative real parts, then the controllable subsystem is stable and the pair (A, B_2) is stabilizable.

Detectability Check: To check if the pair (C_1, A) is detectable, the following steps should be performed:
(I) Firstly, We need to compute the observability matrix of the system defined by (C_1, A), which is given by:

$$Ob = \begin{bmatrix} C_1 \\ C_1 * A \\ C_1 * A^2 \\ \cdots \\ C_1 * A^{n-1} \end{bmatrix} \tag{B.6}$$

where n = 7 is the order of matrix A which is a 7-by-7 matrix.
(II) Secondly, we need to check the rank of the observability matrix. If the rank of Ob matrix is equal to the n, then the pair (C_1, A) is said to be observable. If the rank of Ob is less than n, then we need to use for instance the Kalman decomposition to decompose the system into observable and unobservable subsystems. $Rank(Ob) = 2 < 7$, therefore we need to check if all these five unobservable states are detectable or not. The observable subsystem is given by:

$$A_o = T^{-1}AT = 1.0 \times 10^5 * \begin{bmatrix} -0.0000 & 2.6010 & 0.0000 & 0.0000 & -0.0000 & 0 & -0.0000 \\ -0.0000 & -0.0018 & -0.0000 & 0.0000 & -0.0000 & 0 & -0.0000 \\ 0.0000 & 0.0000 & -0.0002 & -0.8677 & 0.0008 & 0 & 1.2257 \\ -0.0000 & -0.0000 & 0.0000 & -0.0005 & 0.0000 & 0 & 0.0008 \\ -0.0000 & -0.0000 & -0.0000 & 1.2257 & -0.0013 & 0 & -1.7343 \\ 0.0000 & 0.0000 & -0.0000 & 0 & 0.0000 & 0 & 0.0000 \\ -0.0000 & -0.0000 & 0.0000 & 0.0000 & 0.0000 & 0 & 0 \end{bmatrix} \tag{B.7}$$

where T is an observability transformation matrix.
(III) Then, we need to check the eigenvalues of the observable subsystem A_o. If all the eigenvalues of A_o have negative real parts, then the observable subsystem is stable and the pair (C_1, A) is detectable. If any eigenvalue of A_o has a positive real part, then the observable subsystem is unstable and the pair (C_1, A) cannot be detected by any feedback control law.

$$eig(A_o) = 1.0 \times 10^2 * \begin{bmatrix} -0.0000 + 0.0000i \\ -0.1000 + 0.0000i \\ -0.1000 - 0.0000i \\ -0.8965 + 5.0206i \\ -0.8965 - 5.0206i \\ -0.8965 + 5.0206i \\ -0.8965 - 5.0206i \end{bmatrix} \tag{B.8}$$

Therefore, due to all the eigenvalues of A_o having negative real parts, then the observable subsystem is stable and the pair (C_1, A) is detectable.

To check if the pair (C_2, A) is detectable, we should follow the abovementioned steps, therefore, we have: $Rank(Ob) = 4 < 7$, therefore we need to check if all these three unobservable states are detectable or not.

$$A_o = T^{-1}AT = 1.0 \times 10^5 * \begin{bmatrix} -0.0393 & 2.6004 & 0.0000 & -0.0000 & 0.0000 & 0 & 0.0000 \\ -0.0006 & 0.0375 & 0.0000 & 0.0000 & -0.0000 & 0 & -0.0000 \\ -0.0000 & 0.0000 & -0.0002 & -0.8677 & 0.0008 & 0 & 1.2257 \\ 0.0000 & -0.0000 & 0.0000 & -0.0005 & 0.0000 & 0 & 0.0008 \\ -0.0000 & -0.0000 & -0.0000 & 1.2257 & -0.0013 & 0 & -1.7343 \\ 0.0000 & 0.0000 & 0.0000 & 0 & 0 & 0 & 0.0000 \\ 0.0000 & -0.0000 & 0 & 0.0000 & 0.0000 & 0 & 0 \end{bmatrix} \tag{B.9}$$

$$eig(A_o) = 1.0 \times 10^2 * \begin{bmatrix} -0.0000 + 0.0000i \\ -0.8965 + 5.0206i \\ -0.8965 - 5.0206i \\ -0.8965 + 5.0206i \\ -0.8965 - 5.0206i \\ -0.1000 + 0.0000i \\ -0.1000 + 0.0000i \end{bmatrix} \tag{B.10}$$

Therefore, due to all the eigenvalues of A_o having negative real parts, then the observable subsystem is stable and the pair (C_2, A) is detectable.

Proof of the Third Assumption.

$$D_{12}^{T}\begin{bmatrix} C_1 & D_{12}\end{bmatrix} = \begin{bmatrix} 0 & I\end{bmatrix} \tag{B.11}$$

$$\begin{bmatrix} 0 & 0 & 1\end{bmatrix}\begin{bmatrix} 30 & 0 & -30 & 0 & 30 & 0 & 0 & 0\\ 0 & 0 & 0 & 0 & 0 & 0 & 20 & 0\\ 0 & 0 & 0 & 0 & 0 & 0 & 0 & 1\end{bmatrix} = \begin{bmatrix} 0 & 0 & 0 & 0 & 0 & 0 & 0 & 1\end{bmatrix} = \begin{bmatrix} 0 & I\end{bmatrix} \tag{B.12}$$

Appendix C

$\mathbf{K}_{\infty,1}$:

$$A_{k\infty,1} = \begin{bmatrix} -13.8 & -17.88 & -7.127 & -0.8083 & 36.87 & 2.519\\ -22.26 & -78.78 & -139.7 & -5.697 & 4.429 & -11.52\\ -258.7 & -845.3 & -1697 & -112.7 & 4144 & -65.45\\ -10.18 & -175.1 & -95.13 & -1684 & 320 & -26.69\\ 24.81 & 69.14 & 144.2 & -17.37 & -1006 & 84.5\\ -369.3 & -1246 & -2490 & -100.6 & 3614 & -374.3\end{bmatrix} \tag{C.1}$$

$$B_{k\infty,1} = \begin{bmatrix} -66.82 & -2.103\\ -438.1 & 52.15\\ -5491 & -0.6596\\ -373.6 & 1.368\times 10^{4}\\ 518.3 & 354.6\\ -7891 & -30.35\end{bmatrix} \tag{C.2}$$

$$C_{k\infty,1} = \begin{bmatrix} 0.07298 & -0.2474 & -0.1417 & -0.008996 & 0.3294 & 0.02161\end{bmatrix} \tag{C.3}$$

$$D_{k\infty,1} = \begin{bmatrix} -1.235\times 10^{-}20 & -1.907\times 10^{-}22\end{bmatrix} \tag{C.4}$$

References

[1] N. Ertugrul, D. Abbott, DC is the future [Point of view], Proc. IEEE 108 (5) (2020) 615–624, http://dx.doi.org/10.1109/JPROC.2020.2982707.

[2] J.J. Justo, F. Mwasilu, J. Lee, J.-W. Jung, AC-microgrids versus DC-microgrids with distributed energy resources: A review, Renew. Sustain. Energy Rev. 24 (2013) 387–405.

[3] V. Nasirian, S. Moayedi, A. Davoudi, F.L. Lewis, Distributed cooperative control of DC microgrids, IEEE Trans. Power Electron. 30 (4) (2014) 2288–2303.

[4] A. Maknouninejad, Z. Qu, F.L. Lewis, A. Davoudi, Optimal, nonlinear, and distributed designs of droop controls for DC microgrids, IEEE Trans. Smart Grid 5 (5) (2014) 2508–2516, http://dx.doi.org/10.1109/TSG.2014.2325855.

[5] R. Han, M. Tucci, A. Martinelli, J.M. Guerrero, G. Ferrari-Trecate, Stability analysis of primary plug-and-play and secondary leader-based controllers for DC microgrid clusters, IEEE Trans. Power Syst. 34 (3) (2018) 1780–1800.

[6] A. Basati, M.B. Menhaj, A. Fakharian, GA-based optimal droop control approach to improve voltage regulation and equal power sharing for islanded DC microgrids, in: 2016 Electric Power Quality and Supply Reliability, PQ, IEEE, 2016, pp. 145–150.

[7] Q. Shafiee, T. Dragičević, J.C. Vasquez, J.M. Guerrero, Hierarchical control for multiple DC-microgrids clusters, IEEE Trans. Energy Convers. 29 (4) (2014) 922–933.

[8] J.M. Guerrero, J.C. Vasquez, J. Matas, L.G. De Vicuña, M. Castilla, Hierarchical control of droop-controlled AC and DC microgrids—A general approach toward standardization, IEEE Trans. Ind. Electron. 58 (1) (2010) 158–172.

[9] A.A. Mohamed, A.T. Elsayed, T.A. Youssef, O.A. Mohammed, Hierarchical control for DC microgrid clusters with high penetration of distributed energy resources, Electr. Power Syst. Res. 148 (2017) 210–219, http://dx.doi.org/10.1016/j.epsr.2017.04.003, URL: https://www.sciencedirect.com/science/article/pii/S0378779617301505.

[10] Y. Du, X. Lu, W. Tang, Accurate distributed secondary control for DC microgrids considering communication delays: A surplus consensus-based approach, IEEE Trans. Smart Grid 13 (3) (2022) 1709–1719, http://dx.doi.org/10.1109/TSG.2022.3141395.

[11] Y.-Y. Qian, A.V.P. Premakumar, Y. Wan, Z. Lin, Y.A. Shamash, A. Davoudi, Dynamic event-triggered distributed secondary control of DC microgrids, IEEE Trans. Power Electron. 37 (9) (2022) 10226–10238, http://dx.doi.org/10.1109/TPEL.2022.3161967.

[12] J.C. Vasquez, J.M. Guerrero, J. Miret, M. Castilla, L.G. De Vicuna, Hierarchical control of intelligent microgrids, IEEE Ind. Electron. Mag. 4 (4) (2010) 23–29.

[13] F. Gao, R. Kang, J. Cao, T. Yang, Primary and secondary control in DC microgrids: A review, J. Mod. Power Syst. Clean Energy 7 (2) (2019) 227–242.

[14] A. Basati, A. Fakharian, J.M. Guererro, An intelligent droop control for improve voltage regulation and equal power sharing in islanded DC microgrids, in: 2017 5th Iranian Joint Congress on Fuzzy and Intelligent Systems, CFIS, 2017, pp. 190–195, http://dx.doi.org/10.1109/CFIS.2017.8003681.

[15] E. Shahradfar, A. Fakharian, Optimal controller design for DC microgrid based on State-Dependent Riccati Equation (SDRE) approach, Cyber-Phys. Syst. 7 (1) (2021) 41–72.

[16] L. Xing, Q. Xu, F. Guo, Z.-G. Wu, M. Liu, Distributed secondary control for DC microgrid with event-triggered signal transmissions, IEEE Trans. Sustain. Energy 12 (3) (2021) 1801–1810, http://dx.doi.org/10.1109/TSTE.2021.3066334.

[17] A. Basati, J.M. Guerrero, J.C. Vasquez, N. Bazmohammadi, S. Golestan, A data-driven framework for FDI attack detection and mitigation in DC microgrids, Energies 15 (22) (2022) 8539.

[18] M. Tucci, S. Riverso, J.C. Vasquez, J.M. Guerrero, G. Ferrari-Trecate, A decentralized scalable approach to voltage control of DC islanded microgrids, IEEE Trans. Control Syst. Technol. 24 (6) (2016) 1965–1979.

[19] M.S. Sadabadi, Q. Shafiee, A. Karimi, Plug-and-play robust voltage control of DC microgrids, IEEE Trans. Smart Grid 9 (6) (2018) 6886–6896, http://dx.doi.org/10.1109/TSG.2017.2728319.

[20] P. Nahata, R. Soloperto, M. Tucci, A. Martinelli, G. Ferrari-Trecate, A passivity-based approach to voltage stabilization in DC microgrids with ZIP loads, Automatica 113 (2020) 108770, http://dx.doi.org/10.1016/j.automatica.2019.108770, URL: https://www.sciencedirect.com/science/article/pii/S0005109819306338.

[21] T. Bagheri Rouch, A. Fakharian, Robust control of islanded DC microgrid for voltage regulation based on polytopic model and load sharing, Iran. J. Sci. Technol. Trans. Electr. Eng. 46 (1) (2022) 171–186.

[22] N.M. Dehkordi, N. Sadati, M. Hamzeh, Distributed robust finite-time secondary voltage and frequency control of islanded microgrids, IEEE Trans. Power Syst. 32 (5) (2017) 3648–3659, http://dx.doi.org/10.1109/TPWRS.2016.2634085.

[23] B. Ning, Q.-L. Han, L. Ding, Distributed secondary control of AC microgrids with external disturbances and directed communication topologies: A full-order sliding-mode approach, IEEE/CAA J. Autom. Sin. 8 (3) (2021) 554–564, http://dx.doi.org/10.1109/JAS.2020.1003315.

[24] J. Wu, J.M. Guerrero, A. Basati, J.C. Vasquez, S. Li, Kalman filter-based power compensation strategy for microgrids under uncertain disturbance, in: 2022 International Conference on Smart Energy Systems and Technologies, SEST, 2022, pp. 1–5, http://dx.doi.org/10.1109/SEST53650.2022.9898466.

[25] Y. Yin, J. Liu, J.A. Sánchez, L. Wu, S. Vazquez, J.I. Leon, L.G. Franquelo, Observer-based adaptive sliding mode control of NPC converters: An RBF neural network approach, IEEE Trans. Power Electron. 34 (4) (2019) 3831–3841, http://dx.doi.org/10.1109/TPEL.2018.2853093.

[26] A. Basati, J. Wu, J.M. Guerrero, J.C. Vasquez, Internal model-based voltage control for DC microgrids under unknown external disturbances, in: 2022 International Conference on Smart Energy Systems and Technologies, SEST, 2022, pp. 1–6, http://dx.doi.org/10.1109/SEST53650.2022.9898430.

[27] V. Venkatasubramanian, H. Schattler, J. Zaborszky, Fast time-varying phasor analysis in the balanced three-phase large electric power system, IEEE Trans. Automat. Control 40 (11) (1995) 1975–1982, http://dx.doi.org/10.1109/9.471228.

[28] Y. Wang, Z.H. Xiong, H. Ding, Robust internal model control with feedforward controller for a high-speed motion platform, in: 2005 IEEE/RSJ International Conference on Intelligent Robots and Systems, 2005, pp. 187–192, http://dx.doi.org/10.1109/IROS.2005.1545276.

[29] L. Guzzella, C. Onder, Introduction to Modeling and Control of Internal Combustion Engine Systems, Springer Science & Business Media, 2009.

[30] J.C. Smith, G. Hensley, L. Ray, IEEE recommended practice for monitoring electric power quality, 1995, pp. 1159–1995, IEEE Std.

[31] IEEE, IEEE standard for DC microgrids for rural and remote electricity access applications, 2021, pp. 1–47, http://dx.doi.org/10.1109/IEEESTD.2021.9646866, IEEE Std 2030.10-2021.

[32] K. Kaviani, M. Menhaj, A. Fakharian, Mixed H_2/H_∞ state-feedback control for islanded DC microgrids: An LMI based approach, in: 2018 Smart Grid Conference, SGC, 2018, pp. 1–6, http://dx.doi.org/10.1109/SGC.2018.8777886.

[33] J. Doyle, K. Glover, P. Khargonekar, B. Francis, State-space solutions to standard H/sub 2/ and H/sub infinity / control problems, IEEE Trans. Automat. Control 34 (8) (1989) 831–847, http://dx.doi.org/10.1109/9.29425.

[34] P. Gahinet, P. Apkarian, A linear matrix inequality approach to H-infinity control, Internat. J. Robust Nonlinear Control 4 (4) (1994) 421–448.

[35] C.W. Scherer, The Riccati Inequality and State-Space H-Infinity-Optimal Control (Ph.D. thesis), Citeseer, 1990.

[36] S. Skogestad, I. Postlethwaite, Multivariable Feedback Control: Analysis and Design, Vol. 2, Citeseer, 2007.

[37] C. Scherer, P. Gahinet, M. Chilali, Multiobjective output-feedback control via LMI optimization, IEEE Trans. Automat. Control 42 (7) (1997) 896–911, http://dx.doi.org/10.1109/9.599969.

[38] K.J. Åström, T. Hägglund, K.J. Astrom, Advanced PID Control, Vol. 461, ISA-The Instrumentation, Systems, and Automation Society Research Triangle Park, 2006.